






Review

# Recent Developments in Heteroatom/Metal-Doped Carbon Dot-Based Image-Guided Photodynamic Therapy for Cancer

Rajkumar Sekar <sup>1,†</sup>, Nagaraj Basavegowda <sup>2,†</sup>, Saktishree Jena <sup>3</sup>, Santhoshkumar Jayakodi <sup>4</sup>, Pandian Elumalai <sup>4</sup>, Amballa Chaitanyakumar <sup>5</sup>, Prathap Somu <sup>4</sup> and Kwang-Hyun Baek <sup>2,\*</sup>

<sup>1</sup> Department of Chemistry, Karpaga Vinayaga College of Engineering and Technology, GST Road, Chengalpattu 603 308, Tamil Nadu, India

<sup>2</sup> School of Biotechnology, Yeungnam University, Gyeongsan 38541, Korea

<sup>3</sup> Department of Biotechnology, Karpaga Vinayaga College of Engineering and Technology, GST Road, Chengalpattu 603 308, Tamil Nadu, India

<sup>4</sup> Department of Biotechnology, Saveetha Institute of Medical and Technical Sciences (SIMATS), Saveetha School of Engineering, Chennai 602 105, Tamil Nadu, India

<sup>5</sup> Department of Biotechnology, University Institute of Engineering and Technology, Guru Nanak University, Hyderabad 500 085, Telangana, India

\* Correspondence: khbaek@ynu.ac.kr; Tel.: +82-52-810-3029

† These authors contributed equally to this work.

**Abstract:** Carbon nanodots (CNDs) are advanced nanomaterials with a size of 2–10 nm and are considered zero-dimensional carbonaceous materials. CNDs have received great attention in the area of cancer theranostics. The majority of review articles have shown the improvement of CNDs for use in cancer therapy and bioimaging applications. However, there is a minimal number of consolidated studies on the currently developed doped CNDs that are used in various ways in cancer therapies. Hence, in this review, we discuss the current developments in different types of heteroatom elements/metal ion-doped CNDs along with their preparations, physicochemical and biological properties, multimodal-imaging, and emerging applications in image-guided photodynamic therapies for cancer.

**Keywords:** carbon dots; photodynamic therapy; cancer theranostics; bioimaging



**Citation:** Sekar, R.; Basavegowda, N.; Jena, S.; Jayakodi, S.; Elumalai, P.; Chaitanyakumar, A.; Somu, P.; Baek, K.-H. Recent Developments in Heteroatom/Metal-Doped Carbon Dot-Based Image-Guided Photodynamic Therapy for Cancer. *Pharmaceutics* **2022**, *14*, 1869. <https://doi.org/10.3390/pharmaceutics14091869>

Academic Editors: Barbara Tomasello, Irina Naletova and Victor V. Pleshkan

Received: 30 July 2022

Accepted: 25 August 2022

Published: 5 September 2022

**Publisher's Note:** MDPI stays neutral with regard to jurisdictional claims in published maps and institutional affiliations.



**Copyright:** © 2022 by the authors. Licensee MDPI, Basel, Switzerland. This article is an open access article distributed under the terms and conditions of the Creative Commons Attribution (CC BY) license (<https://creativecommons.org/licenses/by/4.0/>).

## 1. Introduction

Cancer is a significant civic health problem, accounting for almost 10 million deaths per annum globally [1–3]. The existing traditional methods for cancers are surgery and chemo/radiotherapy, which have numerous side effects and poor biological barriers [4–6]. For this reason, huge efforts are currently being made to enhance modern approaches with both highly specific therapeutic efficacy and minimal side effects in healthy cells. The near-infrared (NIR)-based photo-ablation therapies comprising photodynamic therapy (PDT) and photothermal therapy (PTT) are emerging as important cancer therapies because of their non-invasive character combined with less cytotoxicity, multi-drug resistance, and minimum harm to healthy cells. Moreover, phototherapies can act together with other modal therapies, namely chemo-, gene-, and immunotherapy, to reduce side effects and develop a supreme way of healing for patients [7–12]. Figure 1 exhibits the mechanisms of photodynamic therapy once the photosensitizers (PSs) have been treated for NIR irradiation with a suitable wavelength range. Initially, electrons are excited from the  $S_0$  (ground state) to the excited  $S_1$  (singlet state) by the absorption of NIR, and then follow the three pathways: (i) return from the  $S_1$  to  $S_0$  via non-radioactive emission in the form of heat, (ii) return from the  $S_1$  to  $S_0$  via radioactive emission, in between the surface trap states present due to surface impurities, defects, and functional groups, and the sub-sequential development of fluorescence, and (iii) conversion starting from the  $S_1$  to the excited  $T_1$  triplet form via intersystem crossing (ISC). Finally, from the  $T_1$  to  $S_0$  ground state, free radicals are

generated via electron transformation to create reactive oxygen species (ROS) [13]. The increasing level of ISC can also increase  $T_1$ , which is useful for sensitizing  $O_2$  to provide  $^1O_2$  and develops the PDT effect [14]. To date, many organic PSs have been reported, namely Phthalocyanine [15], hypocrellin [16,17], and porphyrin [18], which have been utilized in PDT for cancer. Moreover, the reported organic PSs have been restricted due to water insolubility, aggregation, less specificity to tumor cells, and side effects in healthy cells [19–21]. Along with organic PSs, metal and semiconductor-based nanomaterials have been reportedly used in PDT with strong absorbance and expressed high photothermal transfer efficiency. The heavy cytotoxicity of metal ions restricts their usage in clinical trials [22–24]. As a result, the growth of new nanomaterials is necessary for use in PDT for cancer treatment.

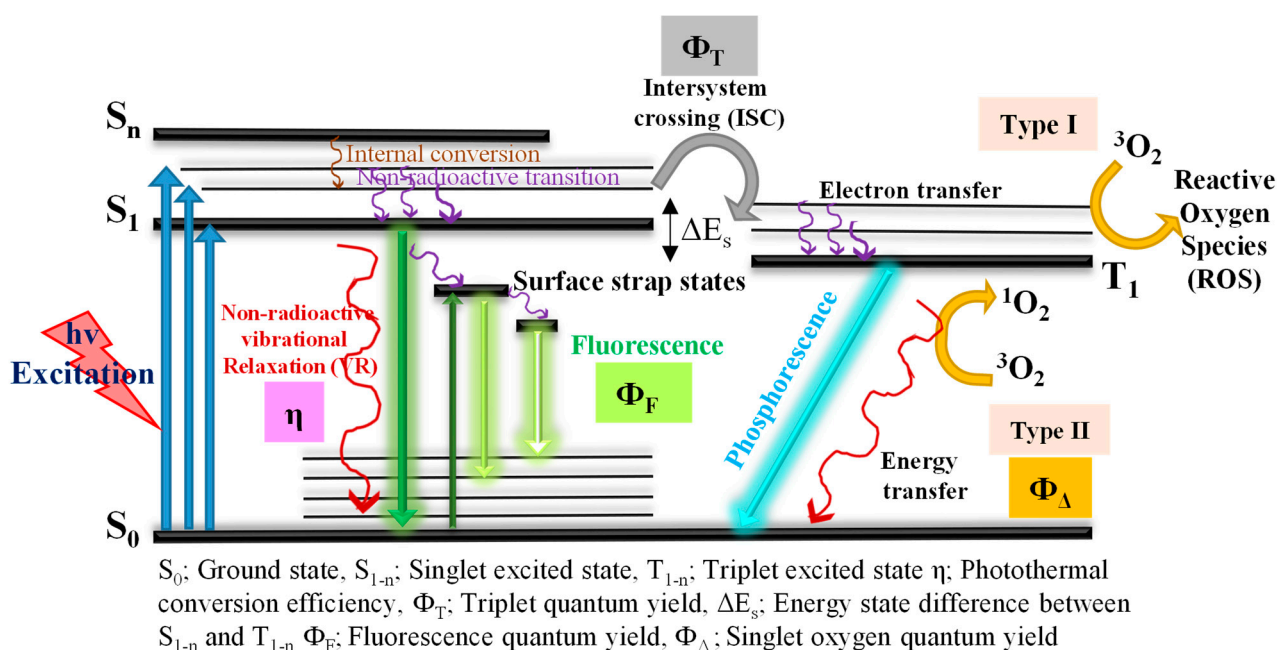


**Figure 1.** The mechanisms of photodynamic therapy.

Carbon nanodots (CNDs) are the new members of the carbon family along with carbon-based nanotubes, diamonds, graphenes, and fibers. CNDs are the latest nanostructure of 0D carbon having a nanosize of 2–10 nm with marvelous luminescent properties [25]. CNDs established with  $sp^2$  hybridized carbon form the core and are surrounded by many functional groups, namely  $-COOH$ ,  $NH$ ,  $OH$ ,  $C-N$ ,  $SH$ , and an aggregation of polymers. CNDs were first discovered accidentally at the time of the refinement of carbon nanotubes by electrophoresis by Xu et al. in 2004 [26]. CNDs have received great interest in the area of biomedical science due to their preparation, quick surface modification ability, unique optical and physicochemical properties, low cytotoxicity, and excitation wavelength of fluorescence and photoluminescence emission [27]. Due to these special characteristics, they have revealed their importance in the area of bio-imaging and biosensors. Moreover, CNDs have the capability to transform NIR energy into ROS and thus can be applied as nanocarriers or PSs in PDT [28–31].

In recent years, many materials scientists have been extensively employing various heteroatoms (fluorine (F), boron (B), phosphorus (P), nitrogen (N), and sulfur (S)) in addition to metals (Ga, Mg, Cu, Zn, Ni, Co, Ca, Au, Fe, etc.) as doping materials to improve the physicochemical properties of CNDs [32–34]. The attachment of metals can modify the electronic structure of CNDs, thereby changing the HOMO–LUMO energy gap on which the optical characteristics of CNDs rest. The luminescent property of CNDs can also be improved because of the surface plasmonic resonance (SPR) nature of metals [35]. In the case of the metal-doped carbon nanodot M-CNDs, surface plasmonic resonance

(SPR) plays a potential role along with the carbon core and the presence of emissive trap states in the surface of M-CNDs. The energy transfer in the M-CNDs causes non-radiative recombination, resulting in enhanced fluorescence quenching. The SPR differs inversely with the ionic size of the metal; the smaller ionic-sized metal ions exhibited higher fluorescence intensity. M-CNDs displayed a surprisingly efficient lifetime due to the SPR-coupled photoluminescence. In heteroatoms, the nitrogen doping of CNDs is the most appreciable strategy for enhancing the CNDs' properties [36]. Consequently, sulfur (S) doping was also established to be beneficial for enhancing the optical properties of CNDs [37]. Other dopants, namely boron (B) [38] and phosphorus (P) [39] have been also used. The development of doped CNDs with heteroatoms/metal ions improves their NIR-induced ROS production rate due to the hopeful photoluminescence and the photo-induced electron transfer properties of CNDs. Currently, numerous review articles have been published on both heteroatom- and metal-doped CNDs and their biomedical applications in cancer therapies. However, no review article has reported on both the metal- and heteroatom-doped CNDs discussing their applications in PDT of cancer alone so far.

In this review, we summarize the recent reports on successful PDT and PDT-based combination therapies based on doped CND-based nanostructures through various surface alterations and fabrication of doped CNDs (Figure 2). This review offers a comprehensive overview of the physicochemical and biological properties of doped CNDs for use in PDT for cancer and how they are altered and fabricated as nanoplatforms for PDT-based cancer therapy.

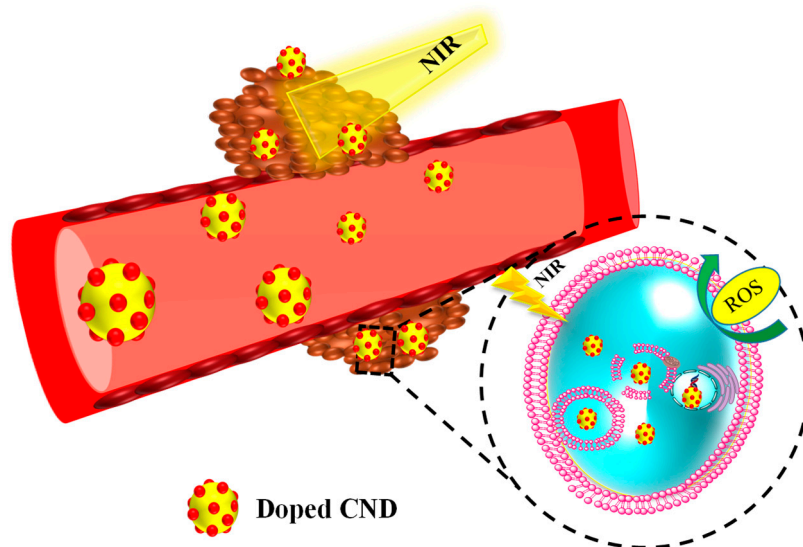


**Figure 2.** Doped CND-based nanostructures for PDT for cancer.

## 2. Synthesis Techniques for Doped CNDs for PDT

Doping is an efficient way to alter the essential properties of CNDs. By presenting heteroatoms/metal ions doped into CNDs, their electronic structures can be altered, promoting n- or p-type carriers. Therefore, their optical and electronic characteristics are linked to the HOMO–LUMO band gaps and they are able to change by using dopants. Additionally, current progress in research has shown that doping could largely improve the quantum yield of CNDs [40]. Commonly, there are two types of methods that can be used to prepare the CNDs, namely top-down and bottom-up methods. Recent methodologies for the synthesis of doped CNDs are summarized in Table 1. In the top-down process, heavy carbon resources (graphite, coal, ash) are decomposed into CNDs, whereas in the bottom-up process, organic matter is converted and polymerized into CNDs [25].

In the top-down process, sulfuric and nitric (strong) acids are employed to oxidize the carbon bulk materials so the surface of CNDs is surrounded by carboxyl and hydroxyl groups [41–43]. The amount of these oxygen-comprising functional groups can be

quickly controlled by tuning the pH range of the acids. Moreover, it is very hard to dope heteroatoms/metal ions into CNDs. Additionally, using strong acids may destroy the  $\pi$ -conjugated forms in the CNDs, as it creates low absorption and low-emission wavelengths. Thus, the top-down process is not adaptable for the large-scale preparation of CNDs. However, in the bottom-up process, CNDs are synthesized using the solvothermal method for the organic substances. Commonly, this is an eco-friendly method using non-toxic solvents and produces a high yield compared to the top-down approach; thus, it is fit for bulky synthesis. The surface functional groups on CNDs are majorly dependent on the chemical formula of carbon materials, pH value, pressure, solvents, and temperature. Different kinds of heteroatoms/metal ions can be quickly doped into CNDs [44]. Furthermore, the doping amount and sites are also hard to regularize. The photoluminescence properties of doped CNDs, particularly their emission and absorption wavelengths, are vital for their photodynamic application in cancer therapies. The doped CNDs with strong NIR fluorescence and absorption can be utilized for successful diagnoses and the destruction of tumors in deep tissue [45].

**Table 1.** Heteroatom/metal-doped CNDs along with their synthesis methods, quantum yields, and colors.

Heteroatom-Doped CNDs					
Synthesis Method	Doping Agent	Precursors	Quantum Yield (%)	Emission	Ref.
Hydrothermal	N	Folic acid	23	Blue	[46]
	F	PEI 600 Da and 2,2,3,3,4,4-hexafluoro-1,5-pentanediol diglycidyl ether	5.6	-	[47]
	P	Sodium citrate and phytic acid	3.5	Blue	[48]
	B	Phenylboronic acid	12	-	[49]
Solvothermal	N	Carbon tetrachloride and diamines	9.8–36.3	Blue	[50]
	F	Tetrafluoroterephthalic acid	-	Green	[51]
	P	Hydroquinone and phosphorous tribromide	25.1	Blue	[39]
	B	Hydroquinone and boron tribromide	14.8	Blue	[52]
Microwave	N	citric acid-malonic acid-oxalic acid-succinic acid	90	Blue	[53]
	P	Ethylenediamine/phytic acid	21.65	Green	[54]
	B	Citric acid, urea, and boric acid	15	Green	[55]
Metal-Doped CNDs					
Hydrothermal	Cu	Poly(methacrylic acid) and Cupric nitrate	80	Blue	[56]
	Zn	Glucose oxidase and glucose, zinc chloride	32.3	Blue	[57]
	Mg, N	Citric acid and Magnesium hydroxide	83	Blue	[58]
	Cu, N	citric acid monohydrate, copper acetate monohydrate	50.1	Blue	[59]
Solvo thermal	Zn	Citric acid monohydrate, urea, zinc chloride	51.2	Yellow	[60]
	Mn	Ethylenediaminetetraacetic acid and manganese chloride tetrahydrate	90.79	Blue	[61]
Micro wave	Fe, N	L-Tartaric acid, urea, FeCl <sub>3</sub> ·6H <sub>2</sub> O, oleic acid	-	Blue	[62]
	Gd	Diethylene glycol (DEG), sucrose, and Gd <sub>2</sub> O <sub>3</sub>	5.4	Green	[63]

### 3. Physicochemical and Biological Properties of Doped CNDs

CNDs as 0D carbon group materials have excellent biocompatibility and their lateral dimensions are typically less than 10 nm [64]. The preparation techniques for doped CNDs are entirely dependent on the approach used (top-down or bottom-up), which have been systematically described [64,65]. Apart from these old-style methods for preparing doped CNDs using carbon sources, currently, many eco-friendly green preparation tactics have been utilized. Well-organized heteroatom/metal-doped CNDs with good hydrophilic properties were prepared by an eco-friendly approach using natural polysaccharides as a precursor [66]. In addition, well-formed heteroatom/metal-doped CNDs have been synthesized with exceptional photoluminescence (optical) and biocompatibility (biological) properties. Furthermore, various advanced techniques in the characterization process have provided a strong underpinning for the usage of doped CNDs in the field of biomedical science.

#### 3.1. Physicochemical Properties of Heteroatom/Metal-Doped CNDs

Most reports confirm that heteroatom/metal doping of CNDs could disturb the pristine electronic structure of CNDs. Thus, the PL properties of doped CNDs are linked to the HOMO–LUMO band gaps that have been changed due to the different types of heteroatom/metal-doped CNDs. The high quantum yield in the doped CNDs enhances the PL properties and also introduces some novel physicochemical properties, namely the magnetic resonance imaging (MRI) relativity rate and catalytic performances. In this section, these physicochemical properties will be exposed and debated.

##### 3.1.1. Photoluminescence in CNDs

The most popular and attractive property of CNDs is its optical (PL) properties since its clear mechanism is still unpredictable. Many proposed mechanisms for CNDs' PL are based on their surface effect, quantum confinement effect, and molecule-like state. In CNDs, a smaller particle size leads to quantum confinement, and many researchers have shown that the energy/band gap of the carbon core energy level increases with the decreasing size of CNDs, subsequently in an emission wavelength with the blue shift of CNDs [67,68]. However, the PL properties arise from the surface effect of the CNDs and develop an improved quantum yield, decay lifetime, and emission wavelength. Many functional groups on CNDs' surface can develop various surface effect energies, which can offer emissive energy levels and create several PL colors [69,70]. Many reported CNDs show blue and green PL emission wavelengths in the range of 400–500 nm; moreover, some red PL emissions have also been observed [71–73]. It is important to note that CNDs with good quantum yields and lifetimes are required in cancer theranostics, particularly to enhance image-guided photodynamic therapy [74].

##### 3.1.2. Photoluminescence in Heteroatom/Metal-Doped CNDs

Heteroatom/metal-doped CNDs showed improved PL properties due to the surface defects via the increasing number of energy traps. Due to this effect, the energy gap of CNDs decreases and the non-radioactive electron transfer has less of an impact and consequently leads to the enhancement of the quantum yield of CNDs [37,70]. In heteroatom doping, the N atom is predominantly used as a dopant and causes a red shift in the emission wavelength of CNDs and an increase in the quantum yield. It can be allocated to the surface energy states created by doping the N onto CNDs, developing a radioactive reunion and reducing the chance of the non-radioactive reunion of excited electrons. Moreover, electron-releasing functional groups such as the amino groups can also increase the excited energy states' stability by improving the pi electrons' conjugation system in the CNDs skeleton. This can improve the electron transition from the ground state to the excited state so the N atom can contribute to the quantum yield of CNDs.

Nowadays, the S atom is also employed as a dopant to improve the quantum yield of CNDs [75,76]. Zhang et al. [77] investigated the electronic structures of carbon dots (CDs), S-doped CDs, and N, S co-doped CDs to describe the high quantum yield of the red and

orange emissions of N, S co-doped CDs. The observed results show that the heteroatoms can create more electronic states and in-gap trap states as recombination points. The heteroatoms (N and S) can quickly bind to carbon owing to their similar atomic radii and the accessibility of the 5 and 6 electrons in their valence band. Thus, N and S doping can alter the band gap of CDs and increase the probability of electronic transition from the singlet ground level to the triplet excited level, concluding in a remarkably high quantum yield of CDs. Similar to the above investigation, Dong et al. [74] analyzed the outcome of N and S co-doped CDs and demonstrated a noteworthy improvement in the quantum yield of S,N co-doped CDs of 73% compared to N-doped CDs with 16.9% and CDs with 5.3%. Moreover, the observed lifetime of N and S co-doped CDs (12.11 ns) was higher than that of non-doped CDs (7.45 ns). The results confirmed that a novel surface energy state formed in CDs through the N-doping method, together with the further co-doping of the S element, can remarkably improve the density of this state. Certainly, the S element can remove the O elements from the surface state and become stable and then improve the surface state of the N element. The optical properties of the doped CNDs are summarized in Table 1.

In recent years, many metal ions have been doped to enhance the luminescence properties of CNDs. The metal doping agents can enhance the quantum yield due to the presence of the valence electron and its electron-transferring processes, which aid the radioactive recombination of holes and electrons on the externally modified surface of the CNDs [32,78,79]. Generally, metal-doped CNDs exhibit a solid and broad absorption band between 200 nm and 600 nm. Compared with CNDs, the emission color of metal-doped CNDs is greatly improved in the visible space at a similar level of concentration owing to the possibility of a charge transfer between the metal dopants and graphite [80,81]. Moreover, most of the metal-doped CNDs show emissions with various colors of fluorescence in a 360 nm UV-vis region, such as yellow [82], green [63], blue [83], blue-green [84], and so on. When compared with CNDs, metal-doped CNDs exhibit a red shift in the fluorescence emission owing to their excitation-based luminescence properties and the emission peaks also demonstrate a higher wavelength with the intensity slowdown as the excitation wavelength exhibits a red shift [56,61,85–88]. Moreover, almost all oxygen-holding functional ligands on the metal-doped CNDs decrease owing to their chemical treatment with the doping metal ions but still show high solubility in aqueous and organic solvents. For instance, Wang et al. [89] showed that the emission fluorescence color of Mn-doped carbon dots changed from blue to yellow as the solvent polarity increased, whereas the emission color of the non-doped CDs was blue with similar solvents and denotes the vital role of Mn doping on CNDs. Heteroatom/metal-doped CNDs can synergistically deliver disease imaging and targeting via PDT, which can be utilized as a new approach for forthcoming cancer theranostics.

### 3.2. Biological Properties of Doped CNDs

Even though the possibilities of using CNDs in nanomedicine are vast, it is essential to study the vital biohazards of CNDs due to the interactions between the CNDs' biomaterials and the body's organs [90–92]. Basically, once CNDs are offered for a particular biomedical use, they must elevate their adequate bio-functions, which can lead to clean renal clearance without side effects [93–95]. Therefore, it is vital to systematically evaluate the toxic nature of heteroatom/metal-doped CNDs from the perspective of toxicology studies. To determine the cytotoxicity *in vitro*, a few biological chemical pointers, namely apoptosis, DNA damage, and reduced oxidative stress, are commonly utilized to fully demonstrate the biocompatibility of heteroatom/metal-doped CNDs with a cell-line medium. Various intravenous processes to introduce CNDs can effectively alter the physiological system and disturb the pharmacokinetics, which depends on the timeline and outcome of the intake, circulation in the bloodstream, metabolic activity, bio-distribution, renal excretion, and bio-interface interaction of superficially introduced CNDs in an organism [96–98].

The quantum yield improvement of doped CNDs is noticeable and important due to the heteroatom/metal doping, which sorts doped CNDs into more convenient biomed-

ical applications. Moreover, the related issue of cytotoxicity caused by the doping of heteroatoms/metals should be observed particularly for their vital role in cancer theranostics applications. Evaluating the cytotoxicity of CNDs through in vitro and in vivo assays to allow for their biomedical applications is necessary for their supplementary advancement. To date, many scientists have assessed the in vitro biocompatibility of different heteroatom/metal-doped CNDs. Commonly, in vitro cytotoxicity models expose cell viability measurements via specific assays namely CCK-8, MTT, and WST-1. Due to their nanosize, which is a major factor affecting their toxicities, CNDs indicate fairly small cytotoxicity in many in vitro models.

Surface-modified CNDs with functional groups, namely  $-NH_2$ ,  $-OH$ ,  $-COOH$ , and heteroatom/metal-doped CNDs, also show low cytotoxicity. Table 2 shows a summary of the biocompatibility experiments of heteroatom/metal-doped CNDs. Many reports have demonstrated the outstanding cell viability of heteroatom-doped CNDs [99–102]. For instance, Edison et al. [103] showed that the nitrogen-doped carbon dots have low cytotoxicity on HeLa cells. Xu et al. [104] achieved a 100% cell viability assay with HeLa and HepG2 cells on doped carbon dots after 24 and 48 h. The biocompatibility reports showed that metal-doped CNDs had low toxicity [83,84,105–111]. For instance, Xu et al. [112] placed an in vivo investigation of Gd-doped carbon dots in liquid form (20 mmol/kg) into mice via a tail vein. After a week of observation, the histological differences in the heart, liver, spleen, kidney, and intestine were analyzed through hematoxylin and eosin staining. In this study, the results showed that there were no significant variations between the control and experiment groups and there were no tissue pathological impairments resulting from the intravenous injection of Gd-doped carbon dots.

**Table 2.** Biocompatibility of doped CNDs.

S. No.	Doped-CND	Cell Model	Assay	Incubation	Viability/Concentration	Ref.
1.	Mg-EDA-CDs	L929	MTT	24 h	90% (250 mg mL <sup>-1</sup> )	[58]
2.	Mn-CDs@Anti-HE4	HO8910	MTS	24 h	85% (3 mg mL <sup>-1</sup> )	[61]
3.	Gd-CDs	C6	MTT	24 h	83% (1 mg mL <sup>-1</sup> )	[63]
4.	Gd-QCDs	NIH3T3	MTT	24 h	121.4 mg mL <sup>-1</sup>	[113]
5.	NPCDs	HepG2	MTT	24 h	88% (100 mg mL <sup>-1</sup> )	[114]
6.	Te-CDs	HeLa	MTT	24 h	80% (200 mg mL <sup>-1</sup> )	[96]
7.	N-O-CDs	HeLa	MTT	24 h	80%	[115]
8.	S, Se-codoped CDs	HeLa	MTT	24 h	>80% (40 mg mL <sup>-1</sup> )	[116]
9.	PMn@Cdots/HA	HEL	WST-1	24 h	100% (20 mg mL <sup>-1</sup> )	[117]
10.	MnNS:CDs@HA	B16F1	WST-1	24 h	90% (500 mg mL <sup>-1</sup> )	[118]

#### 4. Multimodal-Imaging of Doped CNDs

The fluorescent nature of CNDs is very adaptable for direct application in optical imaging. Owing to the occurrence of various emissive levels, CNDs exhibit excitation-based PL. This excitation-based PL property can be utilized to obtain multicolored images of cancer cells. CNDs exhibiting different color emissions with doped elements have been used for fluorescence imaging for PDT. Fluorescence imaging (FI) includes various imaging methods namely, magnetic resonance imaging (MRI), computed X-ray tomography (CT scan), and photoacoustic (PA) imaging, which have different ranges of imaging depths, spatial resolutions, and sensitivities, and all of them are generally applied for the earlier diagnosis of cancer and pre-clinical proposes (Figure 3) Multimodal bio-imaging can combine the benefits of individual imaging modalities, which results in more accurate statistics for therapy design and for guiding therapeutic models [119]. With the aim of enhancing the sensitivity and accuracy of cancer diagnoses, the synthesis of the doped CNDs with multimodal bio-imaging capabilities is highly recommended. General multimodal bio-imaging of CNDs comprises MR/FI, PA/FI, and CT scan/FI.

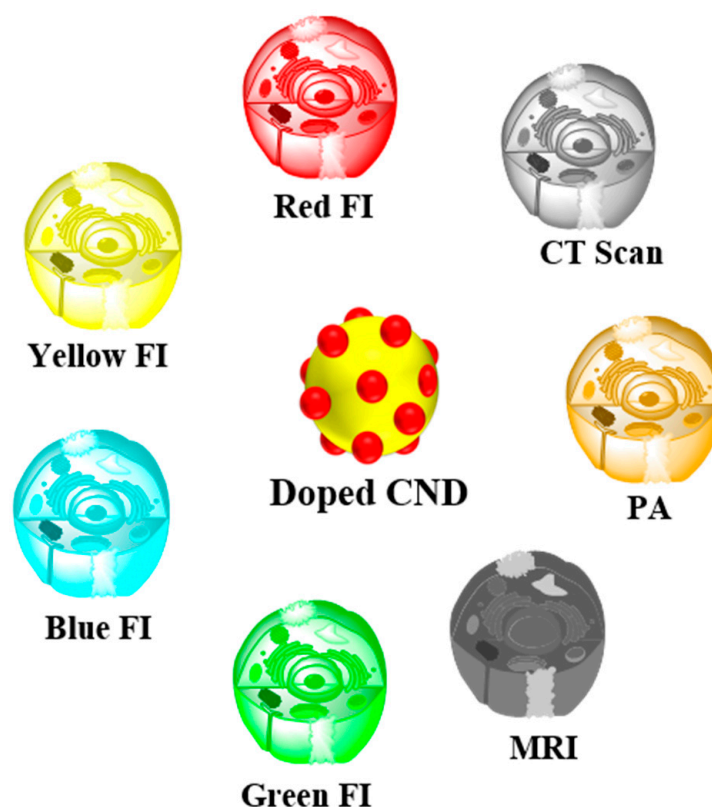


**Figure 3.** Various imaging techniques of heteroatom/metal-doped CNDs.

#### 4.1. MR/FI of Doped CNDs

MR imaging is a non-invasive technique for the early diagnosis and monitoring of diseases during therapy with a high potential for spatial resolution for infected soft tissues. The combination of MR and FI should become an influential non-invasive technique with high spatial resolution and is intensely anticipated [120–122]. In recent years, there have been three classes of MR-based contrast agents such as the paramagnetic metal ligands complex, gadolinium (Gd)- or Mn ( $T_1$ )-based complex, and nanoparticle (iron oxide)  $T_2$ -based contrast agents. The CND-based MR/FI bimodal imaging system can be delivered by the doping of Gd or Mn metal ions into CNDs. Recently, Gd-established complexes have been frequently hybridized with CNDs to generate nanocarriers. In addition,  $Gd^{3+}$  metal ions can be openly doped into CNDs using doping techniques to form Gd-doped CNDs for MR/FI multimodal bio-imaging [123]. Zou et al. synthesized Gd-CDs via the hydrothermal carbonization of gadopentetic acid and glycine. The Gd-CDs exhibited encouraging biocompatibility with good performance at a  $T_1$  relaxivity rate of  $6.45 \text{ mM}^{-1} \text{ s}^{-1}$  and radio sensitization properties, which could be applied to the MR/FI bimodal imaging-guided radio treatment of cancer. Consequently, Gd-doped carbon dots can be used in MR/FI bimodal bio-imaging and decrease the cytotoxicity as well as enhance the longitudinal relativity rate [124].

Wang et al. [125] prepared a Gd-based contrast agent  $Gd@C_{82}$ , which shows a better MRI contrast property than the commercially available Magnevist. The longitudinal relaxivity rate of  $Gd@C_{82}$  and Magnevist in water are  $27 \text{ mM}^{-1} \text{ s}^{-1}$  and  $3.5 \text{ mM}^{-1} \text{ s}^{-1}$  at 7.1 T, respectively. Subsequently, after surface modifications with the  $-OH/NH_2$  group,  $Gd@C_{82}$  can generate a blue light emission under photoexcitation. Moreover, this group of modified  $Gd@C_{82}$  with red emission carbon dots and PEG can enhance the dual-modal bio-imaging and PDT. Wang and Zhang et al. [126] developed boron (B)-doped carbon dots as an alternative  $T_1$  bright agent for use in MRI. The magnetization value of B-CDs was comparatively lower than the well-established Gd-based agents, which offers a new pathway for application in bimodal bio-imaging. On the other hand, Mn-doped CNDs



have also been applied for MR imaging. Wang et al. [127] developed Mn-doped CDs using a hydrothermal process with manganese (II) phthalocyanine. Later, after self-assembly with DSPE-PEG, the formed doped CDs could be employed as a contrast agent for a combined  $T_1$ -weighted MR (relaxivity  $6.97 \text{ mM}^{-1} \text{ s}^{-1}$ )/FI. Gu et al. [128] developed Mn-doped CDs for MR/FI multimodal analysis for blood–brain glioma bio-imaging. Mn-doped CDs exhibited photo-excitation-based emissions and the  $\text{Mn}^{3+}$  metal ions delivered the CDs as a successful  $T_1$ -weighed MR imaging agent.

Further, the Mn-CDs could develop an improved MR contrast effect in the more complex blood–brain glioma sites, which could potentially make them useful in MR/FI multimodal bio-imaging probes to locate blood-brain gliomas. Recently, Han et al. [61] investigated the  $T_1$ -weighed MR contrast imaging of Mn-CDs by inoculating intravenously into HO-8910 cancerous nude mice. From Mn-CDs, the  $T_1$  MR-contrast images were developed at various time intervals. Pre- and post-inoculation results were compared with Mn-CDs on  $T_1$ -weighed signals in the cancer region and improved by 2.06, 2.33, and 2.52 times at 5, 30, and 60 min, respectively. These simultaneous imaging outlines confirmed the gathering of the Mn-CDs in the tumor sites, signifying their importance as a novel type of tumor targeting  $T_1$  MRI contrast agents. Moreover, images of the kidneys could be observed, a sign of the renal clearance of the inoculated Mn-CDs. Luo et al. [129] developed novel liposomal-based carbon dots with iron (Fe@CDs) through self-assemblies of amphiphilic lipopeptides (Figure 4). In this study, Fe@CDs showed good photothermal and gene transfection effects in cancer cells. Furthermore, doped carbon dots could also function as a multimodal imaging agent for PA/PT/MR/FI, exhibiting an order-of-magnitude improvement in the PA signals and  $16^\circ\text{C}$  thermal increases after a 5 min laser treatment on cancer sites.

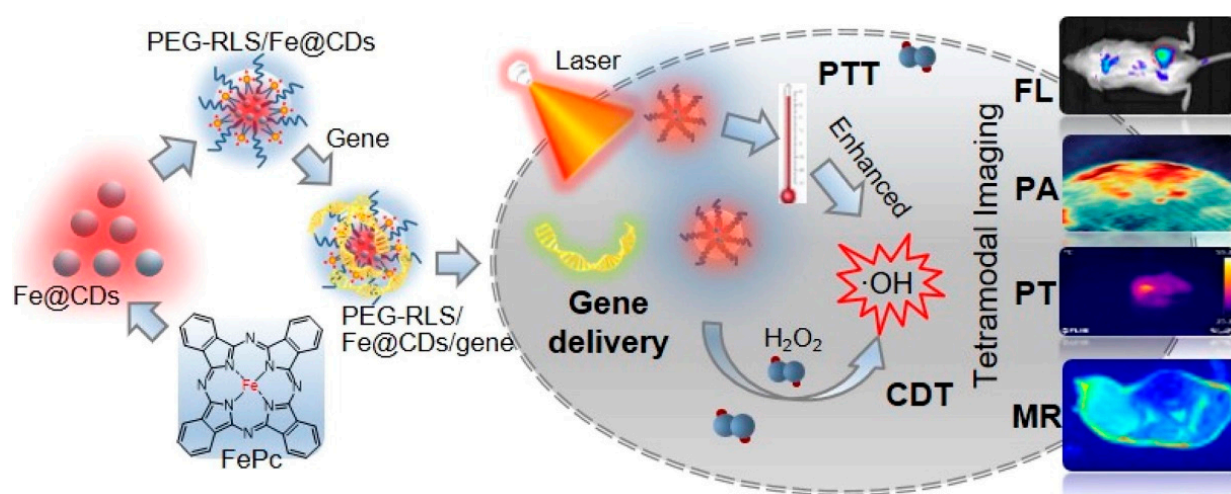


**Figure 4.** Graphical representation of the iron-doped carbon dots as a theranostic agent for PTT, gene delivery, and multimodal (MR/PA/PT/FI) imaging-guided PTT/chemodynamic therapies. Reproduced with permission [129]. Copyright 2021, Elsevier.

#### 4.2. PA/FI of Doped CNDs

Photoacoustic imaging (PAI) is a booming non-invasive imaging technique that can offer an optimized optical contrast and deep imaging of an infected region. When a pulsed laser beam is treated on the nanomaterials it produces isochoric thermal energy, which generates a thermo-elastic explosion as well as ultrasound (US) waves, also named photoacoustic (PA) waves. The PA contrast imaging technique is able to combine optical sensitivity and acoustic depth organ permeation for early disease diagnosis with improved accuracy. Due to their potential photothermal transformation properties, doped CNDs can be utilized as exogenous contrast imaging agents to enhance the PA waves [130–134]. Recently, NIR-triggered cancer theranostics can be applied, which include photodynamics

with real-time photodiagnostics, namely PA and FI, which have been dynamically followed due to their spatiotemporal targeting and specificity for cancer treatment. For instance, Wang et al. [131] synthesized sulfur-doped CDs (SCDs) with red PL by using polythiophene phenylpropionic acid as a precursor. The SCDs can concurrently behave in FI, PA, and photothermal ways for cancer imaging and therapy in pre-clinical mice experiments. The SCDs exhibited a good photothermal conversion proficiency of 38.5%, and the thermal range of the aqueous dispersions increased to 26.6 °C with the accumulation of the SCDs (200 µg/L). The SCDs can gather in organs, such as the kidneys, lungs, and liver, and retain fairly constant PA motion after an extended time circulating in the blood stream during an all-inclusive diagnosis.

The biodistribution of the SCDs in the cancer sites showed improved and flawless PA imaging of cancer regions in mice during pre-clinical studies. Co-doped phosphorus (P) into nitrogen-doped carbon dots (P, N-CDs) can potentially lead to a localized energy state nearer to the Fermi region, thus showing improved PA imaging. The imaging property of P, N-CDs was investigated for in vivo PA and FI using cancerous nude mice as the animal model [133]. Recently, Tian et al. [135] effectively fabricated nickel and nitrogen co-doped carbon dots (Ni-CDs) using a hydrothermal method for imaging-guided phototherapy. The Ni-CDs showed noteworthy absorption in the second near-infrared area with a notable photothermal conversion efficiency of as high as 76.1% under 1064 nm with a power density of 0.5 W cm<sup>-2</sup> and also functioned as PTAs for multimodal PA/MR/PTI-guided photothermal therapy in the second near-infrared area. In this study, in vivo PA and MR imaging of U14 cancerous mice before and after 12 h of an intravenous injection of Ni-CDs were investigated and exhibited thermal increases in the cancerous region of the U14 cancerous mice in the control as well as Ni-CDs with the second near-infrared group under a 1064 nm laser treatment at specific intervals of time.

#### 4.3. CT Scan/FI of Doped CNDs

In addition to the other bio-imaging systems (MRI/FI and PA/FI), computed tomography scanning (CT-scan) is a type of non-invasive imaging used in the clinical diagnosis of diseases [136]. In recent years, Su et al. [137] have fabricated ruthenium-doped carbon dots (Hf-CDs) from thiourea, citric acid, and ruthenium chloride. The prepared Hf-CDs can be successfully applied for the in vivo CT-scan/FI multimodal bio-imaging of orthotopic liver cancer with tumor targeting and active renal clearance. In this study, various organs from mice including kidney, lung, spleen, and liver were forfeited at various durations such as 1, 10, 30, and 60 min post-injection to investigate the distribution and renal clearance of Hf-CDs. Consequently, prepared doped CDs have good targeting capability and noticeable CT-scan/FI processes. Zhang et al. [138] prepared iodine (I)-doped carbon dots (I-CDs) from iodixanol and glycine using a hydrothermal method. The prepared I-CDs exhibited PL emissions of 475 nm and superior X-ray CT. Furthermore, in vivo studies showed that I-CDs were bio-distributed on the infected sites and applied for X-ray CT imaging as well as clean renal clearance. Zhao et al. [139] reported that a novel variety of gadolinium and ytterbium-doped carbon dots were prepared using the hydrothermal method for the multimodal imaging of MR/CT/FI. In this study, the prepared Gd/Yb@CDs exhibited a better CT scan and T<sub>1</sub> MR imaging at (45.43 HU/L g<sup>-1</sup>) and (r<sub>1</sub> = 6.65 mM<sup>-1</sup> s<sup>-1</sup>), respectively. The Gd/Yb@CDs showed optical properties by excitation of the dependent emissions as shown in Figure 5. A summary of the multimodal system of CNDs is presented in Table 3.

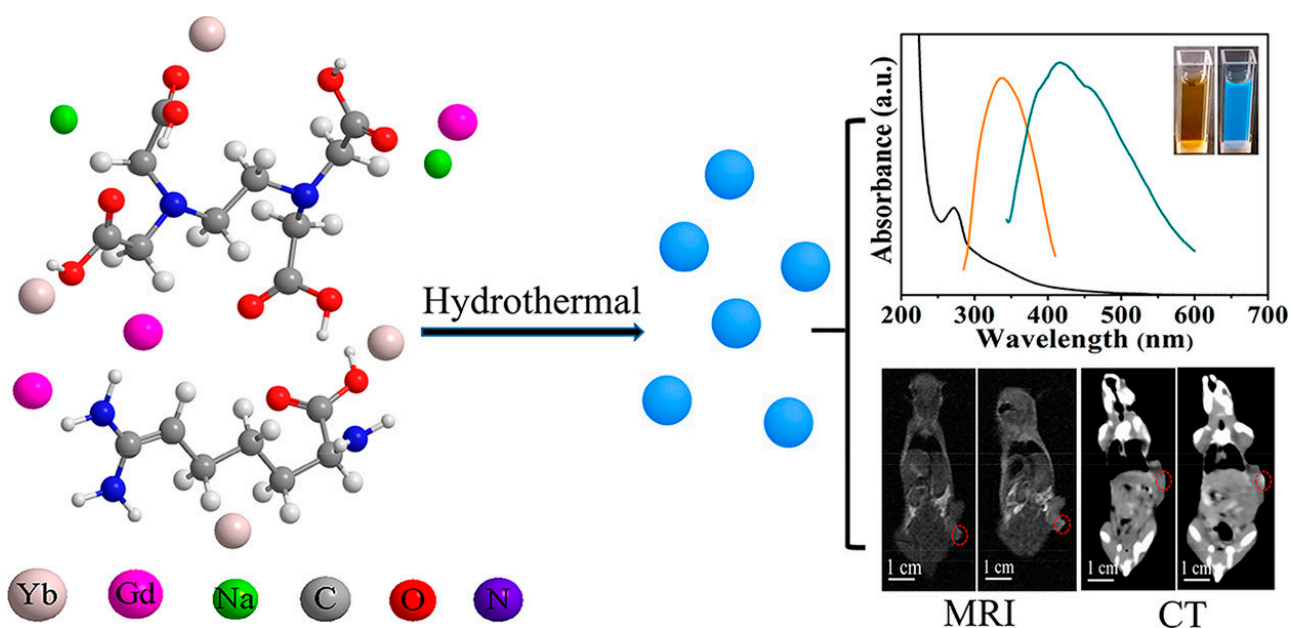


**Figure 5.** Schematic representation of preparation of Gd/Yb@CDs, UV-visible spectrum of doped carbon dots with optical metaphors under 365 nm UV and daylight, and finally, MR and CT images of cancer region observed pre- and post-intravenous administration for 5 h and 24 h, respectively. Reproduced with permission [139]. Copyright 2018, ACS.

**Table 3.** Multimodal imaging properties of heteroatom/metal CNDs.

S. No	Doped CND Materials	Diagnosis Modes	Therapies Applied	Ref.
1.	AS1411-Gd-CDs	MR/FI	PTT	[140]
2.	Dox@IR825@Gd@CDs	MR/FI	CHEMO/PTT	[141]
3.	Se/N-CDs	MR/FI	PTT/PDT	[142]
4.	GNR@SiO <sub>2</sub> -CDs	PA/FI	PTT/PDT	[143]
5.	Gd/Yb@CDs	MR/CT/FI	-	[139]
6.	I-CQDs-C225	CT/FI	-	[144]
7.	Ce6-RCDs	PA/FI	PTT/PDT	[145]
8.	Mn-CDs@Anti-HE4	MR/FI	-	[61]

### 5. Image-Guided Doped CNDs for PDT

PDT has attracted huge attention in basic research, as well as pre-clinical trials, owing to its non-invasive nature, high efficiency against drug resistance, minimal side effects, and minimal damage to the peripheral tissues than currently used cancer therapies. [146–149]. In PDT, the PSs gather in malignant cancer cells and, following laser treatment of PSs by a suitable wavelength, generate ROS from intracellular O<sub>2</sub>, which initiates apoptosis in cancer cells. [150,151]. Thus PSs and photo excitation play vital roles in enhancing PDT. The combination of PSs with doped CNDs can elevate the intracellular uptakes by changing the diffusion mechanism due to their high water solubility, superficial surface modification, good photo stability, biocompatibility, and photon absorption characteristics. Particularly, heteroatom/metal-doped CNDs with a unique nature play a vital role in obtaining ideal PDT cancer theranostic nanomaterials. Moreover, doped CNDs as nanocarriers can realistically be used in image-guided PDT. In this section, we discuss the recently doped CND-based nanocarriers that have emerged for use in PDT, which are dependent on heteroatom- and metal-ion-doped CND nanomaterials as PDT nanoagents.

### 5.1. Image-Guided Metal-Ion-Doped CNDs for PDT

Hu et al. [152] developed innovative and very stable Sn atom-doped carbon dots, which guarantee the effective creation of  $^1\text{O}_2$  (ROS) and improve fluorescence and the PDT effect. In this study, Sn@CDs showed a high quantum yield of 58.3% ( $^1\text{O}_2$ ) with low cytotoxicity on 4T1 cancer cells both in vitro and in vivo, as well as good photoluminescence and water solubility. Furthermore, on irradiation of LED of 400–700 nm with a power density of  $40 \text{ mW/cm}^{-2}$ , a 25% reduction in 4T1 cancer cells with a small impact on healthy cells was observed. Sn@CDs showed that they could reduce tumors and act as good PS, showing a great potential for PDT application. Irmania et al. [153] synthesized amine-functionalized manganese-doped carbon quantum dots (Mn-CQDs). Consequently, folic acid (FA) and chlorin e6 (Ce6) were conjugated to form the Mn-CQDs@FA/Ce6 as a magneto-red photoluminescent property for PDT applications. Mn-CQDs@FA/Ce6 exhibit red PL characteristics at pH 6, 7, and 8 from 0 to 72 h and 7T MRI with a different range of nanomaterial concentrations both in longitudinal ( $1/T_1$ ) and transversal ( $1/T_2$ ) relaxation rates.

In this study, dual-modal imaging and therapy were carried out using Mn-CQDs@FA/Ce6. Their exposed relativity value was 5.77 and they showed a red PL at 360 nm and provided more photodynamic cytotoxicity to HeLa cancer cells via folate-mediated endocytosis. The origin of ROS in cancer cells is vital to the success of PDT. The tumor microenvironment initiating the ROS by Cu- and N-doped carbon dots in mouse melanoma cancer cells suitable for NIR laser treatment with 808 nm utilizing 2',7'-dichlorofluorescein diacetate (DCFH-DA) as a tumor cell penetrable non-emissive agent was investigated. In this experiment, ROS were oxidized by DCFH-DA with outstanding specificity to a deep-green photoluminescent dichlorofluorescein (DCF). The appearance of the emission of green luminescence within mice cancer cells showed the production of  $^1\text{O}_2$  by doped CDs laser treated with 808 nm NIR for 10 min. From these results, the prepared Cu,N-CDs can successfully create  $^1\text{O}_2$  when treated by NIR light in the tumor microenvironment, which can oxidize DCFH-DA, so doped CDs can be used to develop a new photodynamic sensitizer agent. The preparation of a new model of Cu,N-CDs with NIR absorption fitting for combined in vivo PDT and PTT practices is shown in Figure 6 [154].

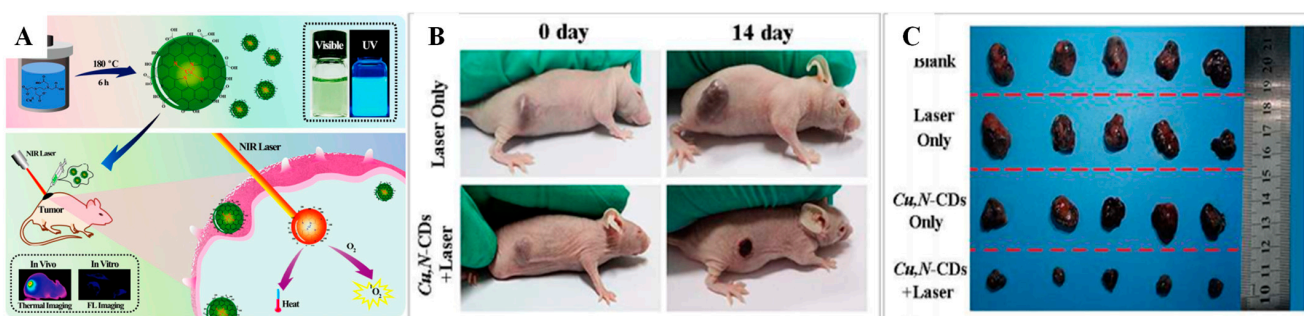


**Figure 6.** (A) Graphical representation of Cu,N-CDs with multimodal theranostics of combined PTT/PDT of mouse melanoma (B16) cells. (B) Photographic images of tumor-bearing mice with laser treatment on different days. (C) Corresponding photographs of tumors in the blank group (Blank without treatment), control groups (only Cu,N-CDs without laser and Laser only applied without Cu,N-CDs), and test group (Cu,N-CDs + Laser). In test group, significant reduction in the tumor size observed, while both control test group (Cu,N-CDs and Laser only) no effect is observed in the tumor size in comparison with blank group. Reproduced with permission [154]. Copyright 2018, Elsevier.

Zheng et al. [155] developed CDs as nanocarriers incorporating cisplatin Pt(IV)-DOX with imageguided therapy against the drug resistance of cisplatin in usual cancer treatment. The successful cellular uptake of the drugs DOX and Pt(IV) was followed by the release of the drugs from their CD nanocarriers under a cancerous cell microenvironment, and then finally, the Pt(IV) and DOX ran their mechanisms to offer a combined therapeutic efficiency

and initiated the successful cell death of A2780 and A2780 cells, which were resilient to Pt(IV). The successful tumor-specific PDT was achieved by constructing nanocarriers to improve oxygenation in the cancer cells of microregions where acidosis and hypoxia, as well as raised levels of  $\text{H}_2\text{O}_2$ , are important. For example, Chen et al. [156], developed CDs/manganese dioxide (CDs/ $\text{MnO}_2$ ) nanocomposites surface-functionalized with PEG to create hydrophilic CDs/ $\text{MnO}_2$ -PEG nanocomposites.

In this study, the developed nanomaterials exhibited fluorescence emission, good  $^1\text{O}_2$  generation, and improved MR imaging in cancer cells. In *in vitro* studies on HeLa cells, the results showed that the acidic environment of cancer cells gave red fluorescence at a  $200 \text{ g mL}^{-1}$  nanomaterial concentration with a 635 nm NIR treatment and induced enhanced apoptosis. On other hand, *in vivo* studies on BALB mice exhibited the effective relief of cancer hypoxia due to the  $\text{MnO}_2$ -stimulated breakdown of hydrogen peroxide into molecular oxygen. This way of improving oxygenation in the tumor microenvironment was a better condition for enhancing the efficiency of image-guided *in vivo* PDT. Thus, the *in vitro* and *in vivo* experiments indicated that the CDs/ $\text{MnO}_2$ -PEG nanocomposites could be used as a pH/ $\text{H}_2\text{O}_2$ -driven, turn-on type of theranostics for multimodal FL/MRI and oxygen-increased PDT for solid cancer therapies. This was also demonstrated by Ge et al. [127] who utilized Mn(II) phthalocyanine to prepare Mn-doped CDs using the solvent thermal method. ROS production by Mn(II)-doped CDs was oxidized via  $\text{H}_2\text{O}_2$  addition, although with the low concentration of oxygen, Mn-doped CDs could generate ROS and molecular oxygen creators to progressively create  $^1\text{O}_2$ . Consequently, this route relocated the triplet energy of PSs to  $\text{O}_2$  to form highly reactive  $^1\text{O}_2$ .

### 5.2. Image-Guided Heteroatom-Doped CNDs for PDT

Owing to their excellent photoelectron transfer behavior, doped CNDs can develop ROS via photoelectron transfer from doped CNDs to molecular oxygen. This advantage can be utilized in PDT, which uses ROS for cancer therapy. In heteroatom-doped CNDs, the ROS generation by nitrogendoped CDs synthesized via the solvothermal transformation of coal resources was investigated, and an  $^1\text{O}_2$  generation with good quantum yield (19.0%) was obtained, which denotes their great importance in PDT [157]. Nitrogendoped carbon dots (NCDs) exhibited both targeting ability and cytotoxicity in tumor cells, showing remarkable inhibition of tumor growths under 630 nm laser irradiation in *in vivo* anticancer therapy. Further, chlorin-e6-conjugated NCDs showed enhanced fluorescence under 430 nm excitation, and a PDT effect on MGC803 cells in the concentration range of 0–50  $\mu\text{M}$  [158]. Zhao et al. [159] developed S and N atom co-doped carbon dots (S,N-CDs) using a hydrothermal method, which resulted in photon fluorescence imaging as well as synergistic photothermal and photodynamic therapies for cancer. In this study, the developed multi-functional heteroatom-doped carbon dots showed that the co-doped (S and N) carbon dots had higher therapeutic efficiency than single doping (N only), and the  $^1\text{O}_2$ -producing ability and photothermal conversion of S,N-CDs was 27%, and 34.4%, respectively. Xu et al. [142] designed selenium- and nitrogendoped carbon dots (Se/N-CDs) as a photosensitizer using RNA as a carrier. In this study, RNA plays a vital role and acts as a carrier and transports the Se/N-CDs close to the nucleus, consequently breaking the nuclear membrane under laser treatment. The prepared Se/N-CDs generated only 10.6% of the  $^1\text{O}_2$ , which is comparatively lower than commercially available photosensitizers.

## 6. Conclusions and Outlook

Heteroatom/metal-doped CNDs as a new member of photoluminescent carbon-family-dependent nanomaterials have excellent potential for use in cancer theranostics owing to their unique physicochemical properties. The fluorescence emission from the UV-visible to near-infrared regions provides the CNDs with the ability to bio-image guided cancer treatment, and thus lead to a pathway for the real-time footprint of bio-distributed drugs on cancer sites. Additionally, heteroatom/metal-doped CNDs have excellent biocompatibility, which reflects the multimodal non-invasive MR/CT/PA imaging potential of doped CNDs.

In this review article, we discussed the current progress and improvements in research in the field of imaging-guided therapy for photodynamic therapy based on heteroatom/metal-doped CNDs, as there were no previous review articles that discussed this subject. This review focused on the outline of the synthesis methodology, physicochemical properties, biocompatibility, multimodal imaging, and finally, the image-guided PDT applications of the heteroatom/metal-doped CNDs. Doped CNDs showed marvelous physicochemical behavior and good ROS production ability and bio-imaging properties, which have often been described as being potential cancer theranostic materials for PDT. The hypoxic nature of tumor delays the molecular oxygen (O<sub>2</sub>)-based PDT method, and the veins of the tumor are demolished after PDT, consequently reducing the O<sub>2</sub> concentration in the tumor site. Moreover, the high hypoxic region may initiate the metastasis of cancer cells. Utilizing the microenvironment sites of the tumor, namely, the hydrogen peroxide, GSH concentrations, and acidic nature of the tumor, leads to an increase in the O<sub>2</sub> in situ, which is vital to clearing the hypoxia problems and enhancing the efficiency of PDT. The physicochemical properties of heteroatom/metal-doped CNDs are linked to their design, composites, and surface interface, and the existing preparation methods for doping CNDs are of comparatively low yield and commonly use natural materials as the source. Moreover, the probable cytotoxicity of heteroatom/metal-doped CNDs reduces their potential uses in clinical trials. The main methods for decreasing the side effects in healthy cells include decreasing the cytotoxicity and proper renal clearance rate of doped CNDs by tuning their size and enhancing the tumortargeting ability. Currently, one of the most basic problems is the lack of a scalable preparation producer to generate high quality doped CNDs with desirable nanostructures (for instance, size, morphology, number of functional groups, and location of defects). Therefore, for the industryscale production of doped CNDs with high performance, the effects of the metal precursors and reaction conditions on the performance of doped CNDs should be systematically explored, and a purification method dependent on size and polarity should also be developed. The enhancement of the PDT enactment of doped CNDs by nano-engineering their unique properties is still a challenging task for materials researchers. Materials scientists should expand the potentially efficient microwave-assisted process owing to their environmentally friendly nature and fast reaction kinetics. Metal-doped CNDs have mostly been used for MR/FI imaging purposes. Therefore, other types of multimodal imaging in the area of Ct scan/FI and PA/FI using exact in vivo models are required. Finally, more effort is needed in the area of image-guided photodynamic therapy using heteroatom/metaldoped CNDs. Even though doped CNDs have had various encounters in pre-clinical trials in PDT due to progress in nanomedicine, the above difficulties will be slowly overcome and it is projected that they will be used for early diagnosis and personalized nanomedicinebased cancer therapy.

**Author Contributions:** Collection of data: S.J. (Saktishree Jena), S.J. (Santhoshkumar Jayakodi), P.E., A.C. and P.S.; writing—original draft preparation: R.S. and N.B.; writing—review and editing: K.-H.B. All authors have read and agreed to the published version of the manuscript.

**Funding:** This research was funded by NRF-2021R1F1A1060297, Basic Science Research Program through the National Research Foundation of Korea (NRF) Ministry of Education.

**Institutional Review Board Statement:** Not applicable.

**Informed Consent Statement:** Not applicable.

**Data Availability Statement:** Not applicable.

**Acknowledgments:** This work was carried out with the support of the Basic Science Research Program through the National Research Foundation of Korea (NRF) funded by the Ministry of Education (NRF-2021R1F1A1060297).

**Conflicts of Interest:** The authors declare no conflict of interest.

## References

1. Yu, Z.; Pan, W.; Li, N.; Tang, B. A nuclear targeted dual-photosensitizer for drug-resistant cancer therapy with NIR activated multiple ROS. *Chem. Sci.* **2016**, *7*, 4237–4244. [[CrossRef](#)] [[PubMed](#)]
2. Wang, Y.; Sun, S.; Zhang, Z.; Shi, D. Nanomaterials for cancer precision medicine. *Adv. Mater.* **2018**, *30*, 1705660. [[CrossRef](#)] [[PubMed](#)]
3. Liu, Y.; Ai, K.; Liu, J.; Deng, M.; He, Y.; Lu, L. Dopamine-Melanin colloidal nanospheres: An efficient near-infrared photothermal therapeutic agent for in vivo cancer therapy. *Adv. Mater.* **2013**, *25*, 1353–1359. [[CrossRef](#)] [[PubMed](#)]
4. Kievit, F.M.; Zhang, M. Surface engineering of iron oxide nanoparticles for targeted cancer therapy. *Acc. Chem. Res.* **2011**, *44*, 853–862. [[CrossRef](#)]
5. Nolsøe, C.P.; Torp-Pedersen, S.; Burcharth, F.; Horn, T.; Pedersen, S.; Christensen, N.E.; Olldag, E.S.; Andersen, P.H.; Karstrup, S.; Lorentzen, T. Interstitial hyperthermia of colorectal liver metastases with a US-guided Nd-YAG laser with a diffuser tip: A pilot clinical study. *Radiology* **1993**, *187*, 333–337. [[CrossRef](#)] [[PubMed](#)]
6. Vogel, A.; Venugopalan, V. Mechanisms of pulsed laser ablation of biological tissues. *Chem. Rev.* **2003**, *103*, 577–644. [[CrossRef](#)]
7. Bhatti, M.; McHugh, T.D.; Milanese, L.; Tomas, S. Self-Assembled nanoparticles as multifunctional drugs for anti-microbial therapies. *Chem. Commun.* **2014**, *50*, 7649–7651. [[CrossRef](#)]
8. Bao, Y.-W.; Hua, X.-W.; Li, Y.-H.; Jia, H.-R.; Wu, F.-G. Hyperthermia-Promoted cytosolic and nuclear delivery of copper/carbon quantum dot-crosslinked nanosheets: Multimodal imaging-guided photothermal cancer therapy. *ACS Appl. Mater. Interfaces* **2018**, *10*, 1544–1555. [[CrossRef](#)]
9. Song, X.; Liang, C.; Gong, H.; Chen, Q.; Wang, C.; Liu, Z. Photosensitizer-Conjugated Albumin—Polypyrrole Nanoparticles for Imaging-Guided In Vivo Photodynamic/Photothermal Therapy. *Small* **2015**, *11*, 3932–3941. [[CrossRef](#)]
10. Lin, J.; Wang, S.; Huang, P.; Wang, Z.; Chen, S.; Niu, G.; Li, W.; He, J.; Cui, D.; Lu, G. Photosensitizer-loaded gold vesicles with strong plasmonic coupling effect for imaging-guided photothermal/photodynamic therapy. *ACS Nano* **2013**, *7*, 5320–5329. [[CrossRef](#)]
11. Zhou, Z.; Song, J.; Tian, R.; Yang, Z.; Yu, G.; Lin, L.; Zhang, G.; Fan, W.; Zhang, F.; Niu, G. Activatable singlet oxygen generation from lipid hydroperoxide nanoparticles for cancer therapy. *Angew. Chem.* **2017**, *129*, 6592–6596. [[CrossRef](#)]
12. Chen, H.; Qiu, Y.; Ding, D.; Lin, H.; Sun, W.; Wang, G.D.; Huang, W.; Zhang, W.; Lee, D.; Liu, G. Gadolinium-Encapsulated graphene carbon nanotheranostics for imaging-guided photodynamic therapy. *Adv. Mater.* **2018**, *30*, 1802748. [[CrossRef](#)] [[PubMed](#)]
13. Yang, D.; Yang, G.; Sun, Q.; Gai, S.; He, F.; Dai, Y.; Zhong, C.; Yang, P. Carbon-Dot-Decorated TiO<sub>2</sub> Nanotubes toward Photodynamic Therapy Based on Water-Splitting Mechanism. *Adv. Healthc. Mater.* **2018**, *7*, 1800042. [[CrossRef](#)] [[PubMed](#)]
14. Kharkwal, G.B.; Sharma, S.K.; Huang, Y.; Dai, T.; Hamblin, M.R. Photodynamic therapy for infections: Clinical applications. *Lasers Surg. Med.* **2011**, *43*, 755–767. [[CrossRef](#)] [[PubMed](#)]
15. Dolmans, D.E.; Fukumura, D.; Jain, R.K. Photodynamic therapy for cancer. *Nat. Rev. Cancer* **2003**, *3*, 380–387. [[CrossRef](#)]
16. Zhang, C.; Wu, J.; Liu, W.; Zheng, X.; Wang, P. Natural-Origin hypocrellin-HSA assembly for highly efficient NIR light-responsive phototheranostics against hypoxic tumors. *ACS Appl. Mater. Interfaces* **2019**, *11*, 44989–44998. [[CrossRef](#)]
17. Ding, Y.; Liu, W.; Wu, J.; Zheng, X.; Ge, J.; Ren, H.; Zhang, W.; Lee, C.; Wang, P. Near-Infrared Hypocrellin Derivatives for Synergistic Photodynamic and Photothermal Therapy. *Chem. Asian J.* **2020**, *15*, 3462–3468. [[CrossRef](#)]
18. Yang, L.; Zhou, J.; Wang, Z.; Li, H.; Wang, K.; Liu, H.; Wu, F. Biocompatible conjugated porphyrin nanoparticles with photodynamic/photothermal performances in cancer therapy. *Dyes Pigments* **2020**, *182*, 108664. [[CrossRef](#)]
19. Lee, C.-S.; Park, W.; Jo, Y.U.; Na, K. A charge-switchable, four-armed polymeric photosensitizer for photodynamic cancer therapy. *Chem. Commun.* **2014**, *50*, 4354–4357. [[CrossRef](#)]
20. Atchison, J.; Kamila, S.; Nesbitt, H.; Logan, K.A.; Nicholas, D.M.; Fowley, C.; Davis, J.; Callan, B.; McHale, A.P.; Callan, J.F. Iodinated cyanine dyes: A new class of sensitizers for use in NIR activated photodynamic therapy (PDT). *Chem. Commun.* **2017**, *53*, 2009–2012. [[CrossRef](#)]
21. Li, D.; Hu, Q.-Y.; Wang, X.-Z.; Li, X.; Hu, J.-Q.; Zheng, B.-Y.; Ke, M.-R.; Huang, J.-D. A non-aggregated silicon (IV) phthalocyanine-lactose conjugate for photodynamic therapy. *Bioorg. Med. Chem. Lett.* **2020**, *30*, 127164. [[CrossRef](#)] [[PubMed](#)]
22. Fernandes, N.; Rodrigues, C.F.; Moreira, A.F.; Correia, I.J. Overview of the application of inorganic nanomaterials in cancer photothermal therapy. *Biomater. Sci.* **2020**, *8*, 2990–3020. [[CrossRef](#)]
23. Lv, S.; Miao, Y.; Liu, D.; Song, F. Recent development of photothermal agents (PTAs) based on small organic molecular dyes. *ChemBioChem* **2020**, *21*, 2098–2110. [[CrossRef](#)] [[PubMed](#)]
24. Samia, A.C.S.; Chen, X.; Burda, C. Semiconductor quantum dots for photodynamic therapy. *J. Am. Chem. Soc.* **2003**, *125*, 15736–15737. [[CrossRef](#)] [[PubMed](#)]
25. Anwar, S.; Ding, H.; Xu, M.; Hu, X.; Li, Z.; Wang, J.; Liu, L.; Jiang, L.; Wang, D.; Dong, C. Recent advances in synthesis, optical properties, and biomedical applications of carbon dots. *ACS Appl. Bio Mater.* **2019**, *2*, 2317–2338. [[CrossRef](#)]
26. Xu, X.; Ray, R.; Gu, Y.; Ploehn, H.J.; Gearheart, L.; Raker, K.; Scrivens, W.A. Electrophoretic analysis and purification of fluorescent single-walled carbon nanotube fragments. *J. Am. Chem. Soc.* **2004**, *126*, 12736–12737. [[CrossRef](#)]
27. Tejwan, N.; Saha, S.K.; Das, J. Multifaceted applications of green carbon dots synthesized from renewable sources. *Adv. Colloid Interface Sci.* **2020**, *275*, 102046. [[CrossRef](#)]

28. Wang, H.; Mukherjee, S.; Yi, J.; Banerjee, P.; Chen, Q.; Zhou, S. Biocompatible chitosan–carbon dot hybrid nanogels for NIR-imaging-guided synergistic photothermal–chemo therapy. *ACS Appl. Mater. Interfaces* **2017**, *9*, 18639–18649. [[CrossRef](#)]
29. Ardekani, S.M.; Dehghani, A.; Hassan, M.; Kianinia, M.; Aharonovich, I.; Gomes, V.G. Two-Photon excitation triggers combined chemo-photothermal therapy via doped carbon nanohybrid dots for effective breast cancer treatment. *Chem. Eng. J.* **2017**, *330*, 651–662. [[CrossRef](#)]
30. Yao, H.; Zhao, W.; Zhang, S.; Guo, X.; Li, Y.; Du, B. Dual-Functional carbon dot-labeled heavy-chain ferritin for self-targeting bio-imaging and chemo-photodynamic therapy. *J. Mater. Chem. B* **2018**, *6*, 3107–3115. [[CrossRef](#)]
31. Zhao, J.; Li, F.; Zhang, S.; An, Y.; Sun, S. Preparation of N-doped yellow carbon dots and N, P co-doped red carbon dots for bioimaging and photodynamic therapy of tumors. *New J. Chem.* **2019**, *43*, 6332–6342. [[CrossRef](#)]
32. Lin, L.; Luo, Y.; Tsai, P.; Wang, J.; Chen, X. Metal ions doped carbon quantum dots: Synthesis, physicochemical properties, and their applications. *TrAC Trends Anal. Chem.* **2018**, *103*, 87–101. [[CrossRef](#)]
33. Zhang, J.; Liu, X.; Wang, X.; Mu, L.; Yuan, M.; Liu, B.; Shi, H. Carbon dots-decorated Na<sub>2</sub>W<sub>4</sub>O<sub>13</sub> composite with WO<sub>3</sub> for highly efficient photocatalytic antibacterial activity. *J. Hazard. Mater.* **2018**, *359*, 1–8. [[CrossRef](#)] [[PubMed](#)]
34. Alonso, M.L.; Montaña, F.P.; Miranda, M.; Castillo, C.; Hernández, J.; Benedito, J.L. Interactions between toxic (As, Cd, Hg and Pb) and nutritional essential (Ca, Co, Cr, Cu, Fe, Mn, Mo, Ni, Se, Zn) elements in the tissues of cattle from NW Spain. *Biomaterials* **2004**, *17*, 389–397. [[CrossRef](#)] [[PubMed](#)]
35. Sajid, P.A.; Chetty, S.S.; Praneetha, S.; Murugan, A.V.; Kumar, Y.; Periyasamy, L. One-Pot microwave-assisted in situ reduction of Ag<sup>+</sup> and Au<sup>3+</sup> ions by Citrus limon extract and their carbon-dots based nanohybrids: A potential nano-bioprobe for cancer cellular imaging. *RSC Adv.* **2016**, *6*, 103482–103490. [[CrossRef](#)]
36. Li, Y.; Zhao, Y.; Cheng, H.; Hu, Y.; Shi, G.; Dai, L.; Qu, L. Nitrogen-Doped graphene quantum dots with oxygen-rich functional groups. *J. Am. Chem. Soc.* **2012**, *134*, 15–18. [[CrossRef](#)]
37. Xu, Q.; Pu, P.; Zhao, J.; Dong, C.; Gao, C.; Chen, Y.; Chen, J.; Liu, Y.; Zhou, H. Preparation of highly photoluminescent sulfur-doped carbon dots for Fe (III) detection. *J. Mater. Chem. A* **2015**, *3*, 542–546. [[CrossRef](#)]
38. Barman, M.K.; Jana, B.; Bhattacharyya, S.; Patra, A. Photophysical properties of doped carbon dots (N, P, and B) and their influence on electron/hole transfer in carbon dots–nickel (II) phthalocyanine conjugates. *J. Phys. Chem. C* **2014**, *118*, 20034–20041. [[CrossRef](#)]
39. Zhou, J.; Shan, X.; Ma, J.; Gu, Y.; Qian, Z.; Chen, J.; Feng, H. Facile synthesis of P-doped carbon quantum dots with highly efficient photoluminescence. *RSC Adv.* **2014**, *4*, 5465–5468. [[CrossRef](#)]
40. Lin, H.; Huang, J.; Ding, L. Preparation of carbon dots with high-fluorescence quantum yield and their application in dopamine fluorescence probe and cellular imaging. *J. Nanomater.* **2019**, *2019*, 5037243. [[CrossRef](#)]
41. Hassan, M.; Gomes, V.G.; Dehghani, A.; Ardekani, S.M. Engineering carbon quantum dots for photomediated theranostics. *Nano Res.* **2018**, *11*, 1–41. [[CrossRef](#)]
42. Jiang, B.; Zhou, B.; Lin, Z.; Liang, H.; Shen, X. Recent advances in carbon nanomaterials for cancer phototherapy. *Chem. Eur. J.* **2019**, *25*, 3993–4004. [[CrossRef](#)] [[PubMed](#)]
43. Du, J.; Xu, N.; Fan, J.; Sun, W.; Peng, X. Carbon dots for in vivo bioimaging and theranostics. *Small* **2019**, *15*, 1805087. [[CrossRef](#)] [[PubMed](#)]
44. Miao, S.; Liang, K.; Zhu, J.; Yang, B.; Zhao, D.; Kong, B. Hetero-Atom-Doped carbon dots: Doping strategies, properties and applications. *Nano Today* **2020**, *33*, 100879. [[CrossRef](#)]
45. Siddique, S.; Chow, J.C.L. Application of nanomaterials in biomedical imaging and cancer therapy. *Nanomaterials* **2020**, *10*, 1700. [[CrossRef](#)]
46. Wang, L.; Yin, Y.; Jain, A.; Zhou, H.S. Aqueous phase synthesis of highly luminescent, nitrogen-doped carbon dots and their application as bioimaging agents. *Langmuir* **2014**, *30*, 14270–14275. [[CrossRef](#)]
47. Luo, T.-Y.; He, X.; Zhang, J.; Chen, P.; Liu, Y.-H.; Wang, H.-J.; Yu, X.-Q. Photoluminescent F-doped carbon dots prepared by ring-opening reaction for gene delivery and cell imaging. *RSC Adv.* **2018**, *8*, 6053–6062. [[CrossRef](#)] [[PubMed](#)]
48. Yang, F.; He, X.; Wang, C.; Cao, Y.; Li, Y.; Yan, L.; Liu, M.; Lv, M.; Yang, Y.; Zhao, X. Controllable and eco-friendly synthesis of P-riched carbon quantum dots and its application for copper (II) ion sensing. *Appl. Surf. Sci.* **2018**, *448*, 589–598. [[CrossRef](#)]
49. Jia, Y.; Hu, Y.; Li, Y.; Zeng, Q.; Jiang, X.; Cheng, Z. Boron doped carbon dots as a multifunctional fluorescent probe for sorbate and vitamin B12. *Microchim. Acta* **2019**, *186*, 84. [[CrossRef](#)]
50. Qian, Z.; Ma, J.; Shan, X.; Feng, H.; Shao, L.; Chen, J. Highly luminescent N-doped carbon quantum dots as an effective multifunctional fluorescence sensing platform. *Chem. Eur. J.* **2014**, *20*, 2254–2263. [[CrossRef](#)]
51. Zuo, G.; Xie, A.; Pan, X.; Su, T.; Li, J.; Dong, W. Fluorine-Doped cationic carbon dots for efficient gene delivery. *ACS Appl. Nano Mater.* **2018**, *1*, 2376–2385. [[CrossRef](#)]
52. Shan, X.; Chai, L.; Ma, J.; Qian, Z.; Chen, J.; Feng, H. B-Doped carbon quantum dots as a sensitive fluorescence probe for hydrogen peroxide and glucose detection. *Analyst* **2014**, *139*, 2322–2325. [[CrossRef](#)] [[PubMed](#)]
53. Meiling, T.T.; Schürmann, R.; Vogel, S.; Ebel, K.; Nicolas, C.; Milosavljević, A.R.; Bald, I. Photophysics and chemistry of nitrogen-doped carbon nanodots with high photoluminescence quantum yield. *J. Phys. Chem. C* **2018**, *122*, 10217–10230. [[CrossRef](#)]
54. Wang, W.; Li, Y.; Cheng, L.; Cao, Z.; Liu, W. Water-Soluble and phosphorus-containing carbon dots with strong green fluorescence for cell labeling. *J. Mater. Chem. B* **2014**, *2*, 46–48. [[CrossRef](#)] [[PubMed](#)]



55. Bourlinos, A.B.; Trivizas, G.; Karakassides, M.A.; Baikousi, M.; Kouloumpis, A.; Gournis, D.; Bakandritsos, A.; Hola, K.; Kozak, O.; Zboril, R. Green and simple route toward boron doped carbon dots with significantly enhanced non-linear optical properties. *Carbon N. Y.* **2015**, *83*, 173–179. [[CrossRef](#)]
56. Ren, X.; Liu, J.; Ren, J.; Tang, F.; Meng, X. One-Pot synthesis of active copper-containing carbon dots with laccase-like activities. *Nanoscale* **2015**, *7*, 19641–19646. [[CrossRef](#)]
57. Xu, Q.; Liu, Y.; Su, R.; Cai, L.; Li, B.; Zhang, Y.; Zhang, L.; Wang, Y.; Wang, Y.; Li, N. Highly fluorescent Zn-doped carbon dots as Fenton reaction-based bio-sensors: An integrative experimental–theoretical consideration. *Nanoscale* **2016**, *8*, 17919–17927. [[CrossRef](#)] [[PubMed](#)]
58. Li, F.; Liu, C.; Yang, J.; Wang, Z.; Liu, W.; Tian, F. Mg/N double doping strategy to fabricate extremely high luminescent carbon dots for bioimaging. *RSC Adv.* **2014**, *4*, 3201–3205. [[CrossRef](#)]
59. Ma, Y.; Cen, Y.; Sohail, M.; Xu, G.; Wei, F.; Shi, M.; Xu, X.; Song, Y.; Ma, Y.; Hu, Q. A ratiometric fluorescence universal platform based on N, Cu codoped carbon dots to detect metabolites participating in H<sub>2</sub>O<sub>2</sub>-generation reactions. *ACS Appl. Mater. Interfaces* **2017**, *9*, 33011–33019. [[CrossRef](#)]
60. Cheng, J.; Wang, C.-F.; Zhang, Y.; Yang, S.; Chen, S. Zinc ion-doped carbon dots with strong yellow photoluminescence. *RSC Adv.* **2016**, *6*, 37189–37194. [[CrossRef](#)]
61. Han, C.; Xu, H.; Wang, R.; Wang, K.; Dai, Y.; Liu, Q.; Guo, M.; Li, J.; Xu, K. Synthesis of a multifunctional manganese (II)–carbon dots hybrid and its application as an efficient magnetic-fluorescent imaging probe for ovarian cancer cell imaging. *J. Mater. Chem. B* **2016**, *4*, 5798–5802. [[CrossRef](#)] [[PubMed](#)]
62. Yang, W.; Huang, T.; Zhao, M.; Luo, F.; Weng, W.; Wei, Q.; Lin, Z.; Chen, G. High peroxidase-like activity of iron and nitrogen co-doped carbon dots and its application in immunosorbent assay. *Talanta* **2017**, *164*, 1–6. [[CrossRef](#)] [[PubMed](#)]
63. Gong, N.; Wang, H.; Li, S.; Deng, Y.; Chen, X.; Ye, L.; Gu, W. Microwave-assisted polyol synthesis of gadolinium-doped green luminescent carbon dots as a bimodal nanoprobe. *Langmuir* **2014**, *30*, 10933–10939. [[CrossRef](#)]
64. Yan, Y.; Gong, J.; Chen, J.; Zeng, Z.; Huang, W.; Pu, K.; Liu, J.; Chen, P. Recent advances on graphene quantum dots: From chemistry and physics to applications. *Adv. Mater.* **2019**, *31*, 1808283. [[CrossRef](#)]
65. Lu, H.; Li, W.; Dong, H.; Wei, M. Graphene quantum dots for optical bioimaging. *Small* **2019**, *15*, 1902136. [[CrossRef](#)] [[PubMed](#)]
66. De Menezes, F.D.; Dos Reis, S.R.R.; Pinto, S.R.; Portilho, F.L.; e Mello, F.D.V.C.; Helal-Neto, E.; De Barros, A.O.D.S.; Alencar, L.M.R.; De Menezes, A.S.; Dos Santos, C.C.; et al. Graphene quantum dots unraveling: Green synthesis, characterization, radiolabeling with <sup>99m</sup>Tc, in vivo behavior and mutagenicity. *Mater. Sci. Eng. C* **2019**, *102*, 405–414. [[CrossRef](#)]
67. Li, H.; He, X.; Kang, Z.; Huang, H.; Liu, Y.; Liu, J.; Lian, S.; Tsang, C.H.A.; Yang, X.; Lee, S. Water-Soluble fluorescent carbon quantum dots and photocatalyst design. *Angew. Chem. Int. Ed.* **2010**, *49*, 4430–4434. [[CrossRef](#)]
68. Kim, S.; Hwang, S.W.; Kim, M.-K.; Shin, D.Y.; Shin, D.H.; Kim, C.O.; Yang, S.B.; Park, J.H.; Hwang, E.; Choi, S.-H. Anomalous behaviors of visible luminescence from graphene quantum dots: Interplay between size and shape. *ACS Nano* **2012**, *6*, 8203–8208. [[CrossRef](#)]
69. Zhu, S.; Song, Y.; Zhao, X.; Shao, J.; Zhang, J.; Yang, B. The photoluminescence mechanism in carbon dots (graphene quantum dots, carbon nanodots, and polymer dots): Current state and future perspective. *Nano Res.* **2015**, *8*, 355–381. [[CrossRef](#)]
70. Yan, F.; Sun, Z.; Zhang, H.; Sun, X.; Jiang, Y.; Bai, Z. The fluorescence mechanism of carbon dots, and methods for tuning their emission color: A review. *Microchim. Acta* **2019**, *186*, 583. [[CrossRef](#)]
71. Zhou, W.; Mo, F.; Sun, Z.; Luo, J.; Fan, J.; Zhu, H.; Zhu, Z.; Huang, J.; Zhang, X. Bright red-emitting P, Br co-doped carbon dots as “OFF-ON” fluorescent probe for Cu<sup>2+</sup> and L-cysteine detection. *J. Alloys Compd.* **2022**, *897*, 162731. [[CrossRef](#)]
72. Sonsin, A.F.; Silva, E.C.O.; Marques, A.L.X.; Silva, L.V.A.T.; Nascimento, S.M.S.; Souza, S.T.; Borbely, A.U.; Barbosa, C.D.E.S.; Fonseca, E.J.S. Tuning the photoluminescence by engineering surface states/size of S, N co-doped carbon dots for cellular imaging applications. *Nanotechnology* **2022**, *33*, 235708. [[CrossRef](#)] [[PubMed](#)]
73. Durrani, S.; Zhang, J.; Yang, Z.; Pang, A.-P.; Zeng, J.; Sayed, S.M.; Khan, A.; Zhang, Y.; Wu, F.-G.; Lin, F. Plant-derived Ca, N, S-Doped carbon dots for fast universal cell imaging and intracellular Congo red detection. *Anal. Chim. Acta* **2022**, *1202*, 339672. [[CrossRef](#)] [[PubMed](#)]
74. Dong, Y.; Pang, H.; Yang, H.B.; Guo, C.; Shao, J.; Chi, Y.; Li, C.M.; Yu, T. Carbon-Based dots co-doped with nitrogen and sulfur for high quantum yield and excitation-independent emission. *Angew. Chem. Int. Ed.* **2013**, *52*, 7800–7804. [[CrossRef](#)] [[PubMed](#)]
75. Wu, F.; Yang, M.; Zhang, H.; Zhu, S.; Zhu, X.; Wang, K. Facile synthesis of sulfur-doped carbon quantum dots from vitamin B1 for highly selective detection of Fe<sup>3+</sup> ion. *Opt. Mater.* **2018**, *77*, 258–263. [[CrossRef](#)]
76. Liu, Y.; Duan, W.; Song, W.; Liu, J.; Ren, C.; Wu, J.; Liu, D.; Chen, H. Red emission B, N, S-co-doped carbon dots for colorimetric and fluorescent dual mode detection of Fe<sup>3+</sup> ions in complex biological fluids and living cells. *ACS Appl. Mater. Interfaces* **2017**, *9*, 12663–12672. [[CrossRef](#)]
77. Zhang, M.; Su, R.; Zhong, J.; Fei, L.; Cai, W.; Guan, Q.; Li, W.; Li, N.; Chen, Y.; Cai, L. Red/orange dual-emissive carbon dots for pH sensing and cell imaging. *Nano Res.* **2019**, *12*, 815–821. [[CrossRef](#)]
78. Xu, Q.; Su, R.; Chen, Y.; Theruvakkattil Sreenivasan, S.; Li, N.; Zheng, X.; Zhu, J.; Pan, H.; Li, W.; Xu, C. Metal charge transfer doped carbon dots with reversibly switchable, ultra-high quantum yield photoluminescence. *ACS Appl. Nano Mater.* **2018**, *1*, 1886–1893. [[CrossRef](#)]
79. Tejwan, N.; Saini, A.K.; Sharma, A.; Singh, T.A.; Kumar, N.; Das, J. Metal-Doped and hybrid carbon dots: A comprehensive review on their synthesis and biomedical applications. *J. Control. Release* **2021**, *330*, 132–150. [[CrossRef](#)]

80. Wu, W.; Zhan, L.; Fan, W.; Song, J.; Li, X.; Li, Z.; Wang, R.; Zhang, J.; Zheng, J.; Wu, M. Cu–N dopants boost electron transfer and photooxidation reactions of carbon dots. *Angew. Chem. Int. Ed.* **2015**, *54*, 6540–6544. [[CrossRef](#)]
81. Zhang, Q.; Xu, W.; Han, C.; Wang, X.; Wang, Y.; Li, Z.; Wu, W.; Wu, M. Graphene structure boosts electron transfer of dual-metal doped carbon dots in photooxidation. *Carbon N. Y.* **2018**, *126*, 128–134. [[CrossRef](#)]
82. Bourlinos, A.B.; Rathi, A.K.; Gawande, M.B.; Hola, K.; Goswami, A.; Kalytchuk, S.; Karakassides, M.A.; Kouloumpis, A.; Gournis, D.; Deligiannakis, Y. Fe (III)-functionalized carbon dots—Highly efficient photoluminescence redox catalyst for hydrogenations of olefins and decomposition of hydrogen peroxide. *Appl. Mater. Today* **2017**, *7*, 179–184. [[CrossRef](#)]
83. Liao, H.; Wang, Z.; Chen, S.; Wu, H.; Ma, X.; Tan, M. One-pot synthesis of gadolinium (III) doped carbon dots for fluorescence/magnetic resonance bimodal imaging. *RSC Adv.* **2015**, *5*, 66575–66581. [[CrossRef](#)]
84. Yuan, Y.H.; Li, R.S.; Wang, Q.; Wu, Z.L.; Wang, J.; Liu, H.; Huang, C.Z. Germanium-Doped carbon dots as a new type of fluorescent probe for visualizing the dynamic invasions of mercury (II) ions into cancer cells. *Nanoscale* **2015**, *7*, 16841–16847. [[CrossRef](#)]
85. Wang, Y.; Zhang, Y.; Jia, M.; Meng, H.; Li, H.; Guan, Y.; Feng, L. Functionalization of carbonaceous nanodots from MnII-coordinating functional knots. *Chem. Eur. J.* **2015**, *21*, 14843–14850. [[CrossRef](#)]
86. Zhu, C.; Yang, S.; Sun, J.; He, P.; Yuan, N.; Ding, J.; Mo, R.; Wang, G.; Ding, G.; Xie, X. Deep ultraviolet emission photoluminescence and high luminescence efficiency of ferric passivated graphene quantum dots: Strong negative inductive effect of Fe. *Synth. Met.* **2015**, *209*, 468–472. [[CrossRef](#)]
87. Lin, L.; Song, X.; Chen, Y.; Rong, M.; Wang, Y.; Zhao, L.; Zhao, T.; Chen, X. Europium-decorated graphene quantum dots as a fluorescent probe for label-free, rapid and sensitive detection of Cu<sup>2+</sup> and L-cysteine. *Anal. Chim. Acta* **2015**, *891*, 261–268. [[CrossRef](#)]
88. Liu, T.; Li, N.; Dong, J.X.; Luo, H.Q.; Li, N.B. Fluorescence detection of mercury ions and cysteine based on magnesium and nitrogen co-doped carbon quantum dots and IMPLICATION logic gate operation. *Sens. Actuators B Chem.* **2016**, *231*, 147–153. [[CrossRef](#)]
89. Wang, Y.; Meng, H.; Jia, M.; Zhang, Y.; Li, H.; Feng, L. Intraparticle FRET of Mn (ii)-doped carbon dots and its application in discrimination of volatile organic compounds. *Nanoscale* **2016**, *8*, 17190–17195. [[CrossRef](#)]
90. Peng, Z.; Han, X.; Li, S.; Al-Youbi, A.O.; Bashammakh, A.S.; El-Shahawi, M.S.; Leblanc, R.M. Carbon dots: Biomacromolecule interaction, bioimaging and nanomedicine. *Coord. Chem. Rev.* **2017**, *343*, 256–277. [[CrossRef](#)]
91. Liu, Y.-Y.; Yu, N.-Y.; Fang, W.-D.; Tan, Q.-G.; Ji, R.; Yang, L.-Y.; Wei, S.; Zhang, X.-W.; Miao, A.-J. Photodegradation of carbon dots cause cytotoxicity. *Nat. Commun.* **2021**, *12*, 812. [[CrossRef](#)] [[PubMed](#)]
92. Liang, X.; Li, N.; Zhang, R.; Yin, P.; Zhang, C.; Yang, N.; Liang, K.; Kong, B. Carbon-Based SERS biosensor: From substrate design to sensing and bioapplication. *NPG Asia Mater.* **2021**, *13*, 8. [[CrossRef](#)]
93. Li, N.; Than, A.; Sun, C.; Tian, J.; Chen, J.; Pu, K.; Dong, X.; Chen, P. Monitoring dynamic cellular redox homeostasis using fluorescence-switchable graphene quantum dots. *ACS Nano* **2016**, *10*, 11475–11482. [[CrossRef](#)]
94. Li, F.; Li, Y.; Yang, X.; Han, X.; Jiao, Y.; Wei, T.; Yang, D.; Xu, H.; Nie, G. Highly fluorescent chiral N-S-doped carbon dots from cysteine: Affecting cellular energy metabolism. *Angew. Chem.* **2018**, *130*, 2401–2406. [[CrossRef](#)]
95. Song, Y.; Wu, Y.; Wang, H.; Liu, S.; Song, L.; Li, S.; Tan, M. Carbon quantum dots from roasted Atlantic salmon (*Salmo salar* L.): Formation, biodistribution and cytotoxicity. *Food Chem.* **2019**, *293*, 387–395. [[CrossRef](#)] [[PubMed](#)]
96. Chen, H.; Wen, K.; Chen, J.; Xing, W.; Wu, X.; Shi, Q.; Peng, A.; Huang, H. Ultra-Stable tellurium-doped carbon quantum dots for cell protection and near-infrared photodynamic application. *Sci. Bull.* **2020**, *65*, 1580–1586. [[CrossRef](#)]
97. Wang, S.; Cole, I.S.; Li, Q. The toxicity of graphene quantum dots. *RSC Adv.* **2016**, *6*, 89867–89878. [[CrossRef](#)]
98. Mishra, V.; Patil, A.; Thakur, S.; Kesharwani, P. Carbon dots: Emerging theranostic nanoarchitectures. *Drug Discov. Today* **2018**, *23*, 1219–1232. [[CrossRef](#)]
99. Li, J.; Zuo, G.; Pan, X.; Wei, W.; Qi, X.; Su, T.; Dong, W. Nitrogen-Doped carbon dots as a fluorescent probe for the highly sensitive detection of Ag<sup>+</sup> and cell imaging. *Luminescence* **2018**, *33*, 243–248. [[CrossRef](#)]
100. Zhang, Q.; Xie, S.; Yang, Y.; Wu, Y.; Wang, X.; Wu, J.; Zhang, L.; Chen, J.; Wang, Y. A facile synthesis of highly nitrogen-doped carbon dots for imaging and detection in biological samples. *J. Anal. Methods Chem.* **2018**, *2018*, 7890937. [[CrossRef](#)]
101. Arul, V.; Edison, T.N.J.I.; Lee, Y.R.; Sethuraman, M.G. Biological and catalytic applications of green synthesized fluorescent N-doped carbon dots using *Hylocereus undatus*. *J. Photochem. Photobiol. B Biol.* **2017**, *168*, 142–148. [[CrossRef](#)] [[PubMed](#)]
102. Edison, T.N.J.I.; Atchudan, R.; Shim, J.-J.; Kalimuthu, S.; Ahn, B.-C.; Lee, Y.R. Turn-Off fluorescence sensor for the detection of ferric ion in water using green synthesized N-doped carbon dots and its bio-imaging. *J. Photochem. Photobiol. B Biol.* **2016**, *158*, 235–242. [[CrossRef](#)] [[PubMed](#)]
103. Edison, T.N.J.I.; Atchudan, R.; Sethuraman, M.G.; Shim, J.-J.; Lee, Y.R. Microwave assisted green synthesis of fluorescent N-doped carbon dots: Cytotoxicity and bio-imaging applications. *J. Photochem. Photobiol. B Biol.* **2016**, *161*, 154–161. [[CrossRef](#)] [[PubMed](#)]
104. Xu, Y.; Wu, M.; Liu, Y.; Feng, X.; Yin, X.; He, X.; Zhang, Y. Nitrogen-Doped carbon dots: A facile and general preparation method, photoluminescence investigation, and imaging applications. *Chem. Eur. J.* **2013**, *19*, 2276–2283. [[CrossRef](#)]
105. Chen, H.; Wang, G.D.; Tang, W.; Todd, T.; Zhen, Z.; Tsang, C.; Hekmatyar, K.; Cowger, T.; Hubbard, R.B.; Zhang, W. Gd-Encapsulated carbonaceous dots with efficient renal clearance for magnetic resonance imaging. *Adv. Mater.* **2014**, *26*, 6761–6766. [[CrossRef](#)]

106. Ren, X.; Liu, L.; Li, Y.; Dai, Q.; Zhang, M.; Jing, X. Facile preparation of gadolinium (iii) chelates functionalized carbon quantum dot-based contrast agent for magnetic resonance/fluorescence multimodal imaging. *J. Mater. Chem. B* **2014**, *2*, 5541–5549. [[CrossRef](#)]
107. Chen, H.; Wang, G.D.; Sun, X.; Todd, T.; Zhang, F.; Xie, J.; Shen, B. Mesoporous silica as nanoreactors to prepare Gd-encapsulated carbon dots of controllable sizes and magnetic properties. *Adv. Funct. Mater.* **2016**, *26*, 3973–3982. [[CrossRef](#)]
108. Pan, Y.; Yang, J.; Fang, Y.; Zheng, J.; Song, R.; Yi, C. One-Pot synthesis of gadolinium-doped carbon quantum dots for high-performance multimodal bioimaging. *J. Mater. Chem. B* **2017**, *5*, 92–101. [[CrossRef](#)]
109. Shi, Y.; Pan, Y.; Zhong, J.; Yang, J.; Zheng, J.; Cheng, J.; Song, R.; Yi, C. Facile synthesis of gadolinium (III) chelates functionalized carbon quantum dots for fluorescence and magnetic resonance dual-modal bioimaging. *Carbon N. Y.* **2015**, *93*, 742–750. [[CrossRef](#)]
110. Ren, X.Y.; Yuan, X.X.; Wang, Y.P.; Liu, C.L.; Qin, Y.; Guo, L.P.; Liu, L.H. Facile preparation of Gd<sup>3+</sup> doped carbon quantum dots: Photoluminescence materials with magnetic resonance response as magnetic resonance/fluorescence bimodal probes. *Opt. Mater.* **2016**, *57*, 56–62. [[CrossRef](#)]
111. Yu, C.; Xuan, T.; Chen, Y.; Zhao, Z.; Liu, X.; Lian, G.; Li, H. Gadolinium-Doped carbon dots with high quantum yield as an effective fluorescence and magnetic resonance bimodal imaging probe. *J. Alloys Compd.* **2016**, *688*, 611–619. [[CrossRef](#)]
112. Xu, Y.; Jia, X.-H.; Yin, X.-B.; He, X.-W.; Zhang, Y.-K. Carbon quantum dot stabilized gadolinium nanoprobe prepared via a one-pot hydrothermal approach for magnetic resonance and fluorescence dual-modality bioimaging. *Anal. Chem.* **2014**, *86*, 12122–12129. [[CrossRef](#)] [[PubMed](#)]
113. Bourlinos, A.B.; Bakandritsos, A.; Kouloumpis, A.; Gournis, D.; Krysmann, M.; Giannelis, E.P.; Polakova, K.; Safarova, K.; Hola, K.; Zboril, R. Gd (III)-doped carbon dots as a dual fluorescent-MRI probe. *J. Mater. Chem.* **2012**, *22*, 23327–23330. [[CrossRef](#)]
114. Yang, X.; Zhang, M.; Zhang, Y.; Wang, N.; Bian, W.; Choi, M.M.F. Nitrogen and phosphorus co-doped carbon dots as a “turn-off-on” fluorescence probe for the detection of Hg<sup>2+</sup> and GSH and cell imaging. *Anal. Methods* **2019**, *11*, 5803–5809. [[CrossRef](#)]
115. Geng, B.; Yang, D.; Pan, D.; Wang, L.; Zheng, F.; Shen, W.; Zhang, C.; Li, X. NIR-Responsive carbon dots for efficient photothermal cancer therapy at low power densities. *Carbon N. Y.* **2018**, *134*, 153–162. [[CrossRef](#)]
116. Lan, M.; Zhao, S.; Zhang, Z.; Yan, L.; Guo, L.; Niu, G.; Zhang, J.; Zhao, J.; Zhang, H.; Wang, P. Two-Photon-Excited near-infrared emissive carbon dots as multifunctional agents for fluorescence imaging and photothermal therapy. *Nano Res.* **2017**, *10*, 3113–3123. [[CrossRef](#)]
117. Lin, J.-S.; Tsai, Y.-W.; Dehvari, K.; Huang, C.-C.; Chang, J.-Y. A carbon dot based theranostic platform for dual-modal imaging and free radical scavenging. *Nanoscale* **2019**, *11*, 20917–20931. [[CrossRef](#)]
118. Dehvari, K.; Chiu, S.-H.; Lin, J.-S.; Girma, W.M.; Ling, Y.-C.; Chang, J.-Y. Heteroatom doped carbon dots with nanoenzyme like properties as theranostic platforms for free radical scavenging, imaging, and chemotherapy. *Acta Biomater.* **2020**, *114*, 343–357. [[CrossRef](#)]
119. Li, W.; Zheng, C.; Pan, Z.; Chen, C.; Hu, D.; Gao, G.; Kang, S.; Cui, H.; Gong, P.; Cai, L. Smart hyaluronidase-activated theranostic micelles for dual-modal imaging guided photodynamic therapy. *Biomaterials* **2016**, *101*, 10–19. [[CrossRef](#)]
120. Santra, S.; Kaittanis, C.; Grimm, J.; Perez, J.M. Drug/Dye-Loaded, multifunctional iron oxide nanoparticles for combined targeted cancer therapy and dual optical/magnetic resonance imaging. *Small* **2009**, *5*, 1862–1868. [[CrossRef](#)]
121. Yin, M.; Li, Z.; Liu, Z.; Ren, J.; Yang, X.; Qu, X. Photosensitizer-incorporated G-quadruplex DNA-functionalized magnetofluorescent nanoparticles for targeted magnetic resonance/fluorescence multimodal imaging and subsequent photodynamic therapy of cancer. *Chem. Commun.* **2012**, *48*, 6556–6558. [[CrossRef](#)] [[PubMed](#)]
122. Chen, W.-H.; Luo, G.-F.; Lei, Q.; Cao, F.-Y.; Fan, J.-X.; Qiu, W.-X.; Jia, H.-Z.; Hong, S.; Fang, F.; Zeng, X. Rational design of multifunctional magnetic mesoporous silica nanoparticle for tumor-targeted magnetic resonance imaging and precise therapy. *Biomaterials* **2016**, *76*, 87–101. [[CrossRef](#)] [[PubMed](#)]
123. Gedda, G.; Yao, Y.-Y.; Chen, S.-H.; Ghule, A.V.; Ling, Y.-C.; Chang, J.-Y. Facile synthesis of gold/gadolinium-doped carbon quantum dot nanocomposites for magnetic resonance imaging and photothermal ablation therapy. *J. Mater. Chem. B* **2017**, *5*, 6282–6291. [[CrossRef](#)] [[PubMed](#)]
124. Du, F.; Zhang, L.; Zhang, L.; Zhang, M.; Gong, A.; Tan, Y.; Miao, J.; Gong, Y.; Sun, M.; Ju, H. Engineered gadolinium-doped carbon dots for magnetic resonance imaging-guided radiotherapy of tumors. *Biomaterials* **2017**, *121*, 109–120. [[CrossRef](#)]
125. Wang, F.H.; Bae, K.; Huang, Z.W.; Xue, J.M. Two-Photon graphene quantum dot modified Gd<sub>2</sub>O<sub>3</sub> nanocomposites as a dual-mode MRI contrast agent and cell labelling agent. *Nanoscale* **2018**, *10*, 5642–5649. [[CrossRef](#)] [[PubMed](#)]
126. Wang, H.; Revia, R.; Wang, K.; Kant, R.J.; Mu, Q.; Gai, Z.; Hong, K.; Zhang, M. Paramagnetic properties of metal-free boron-doped graphene quantum dots and their application for safe magnetic resonance imaging. *Adv. Mater.* **2017**, *29*, 1605416. [[CrossRef](#)]
127. Jia, Q.; Ge, J.; Liu, W.; Zheng, X.; Chen, S.; Wen, Y.; Zhang, H.; Wang, P. A magnetofluorescent carbon dot assembly as an acidic H<sub>2</sub>O<sub>2</sub>-driven oxygenerator to regulate tumor hypoxia for simultaneous bimodal imaging and enhanced photodynamic therapy. *Adv. Mater.* **2018**, *30*, 1706090. [[CrossRef](#)]
128. Ji, Z.; Ai, P.; Shao, C.; Wang, T.; Yan, C.; Ye, L.; Gu, W. Manganese-Doped carbon dots for magnetic resonance/optical dual-modal imaging of tiny brain glioma. *ACS Biomater. Sci. Eng.* **2018**, *4*, 2089–2094. [[CrossRef](#)] [[PubMed](#)]
129. Luo, T.; Nie, Y.; Lu, J.; Bi, Q.; Cai, Z.; Song, X.; Ai, H.; Jin, R. Iron doped carbon dots based nanohybrids as a tetramodal imaging agent for gene delivery promotion and photothermal-chemodynamic cancer synergistic theranostics. *Mater. Des.* **2021**, *208*, 109878. [[CrossRef](#)]

130. Zackrisson, S.; Van De Ven, S.; Gambhir, S.S. Light In and Sound Out: Emerging Translational Strategies for Photoacoustic Imaging—Translational Strategies for Photoacoustic Imaging. *Cancer Res.* **2014**, *74*, 979–1004. [[CrossRef](#)]
131. Ge, J.; Jia, Q.; Liu, W.; Guo, L.; Liu, Q.; Lan, M.; Zhang, H.; Meng, X.; Wang, P. Red-Emissive carbon dots for fluorescent, photoacoustic, and thermal theranostics in living mice. *Adv. Mater.* **2015**, *27*, 4169–4177. [[CrossRef](#)] [[PubMed](#)]
132. Wu, L.; Cai, X.; Nelson, K.; Xing, W.; Xia, J.; Zhang, R.; Stacy, A.J.; Luderer, M.; Lanza, G.M.; Wang, L.V. A green synthesis of carbon nanoparticles from honey and their use in real-time photoacoustic imaging. *Nano Res.* **2013**, *6*, 312–325. [[CrossRef](#)] [[PubMed](#)]
133. Parvin, N.; Mandal, T.K. Dually emissive P, N-co-doped carbon dots for fluorescent and photoacoustic tissue imaging in living mice. *Microchim. Acta* **2017**, *184*, 1117–1125. [[CrossRef](#)]
134. Lee, C.; Kwon, W.; Beack, S.; Lee, D.; Park, Y.; Kim, H.; Hahn, S.K.; Rhee, S.-W.; Kim, C. Biodegradable nitrogen-doped carbon nanodots for non-invasive photoacoustic imaging and photothermal therapy. *Theranostics* **2016**, *6*, 2196. [[CrossRef](#)]
135. Tian, B.; Liu, S.; Feng, L.; Liu, S.; Gai, S.; Dai, Y.; Xie, L.; Liu, B.; Yang, P.; Zhao, Y. Renal-Clearable nickel-doped carbon dots with boosted photothermal conversion efficiency for multimodal imaging-guided cancer therapy in the second near-infrared biowindow. *Adv. Funct. Mater.* **2021**, *31*, 2100549. [[CrossRef](#)]
136. Rajkumar, S.; Prabaharan, M. Theranostics based on iron oxide and gold nanoparticles for imaging-guided photothermal and photodynamic therapy of cancer. *Curr. Top. Med. Chem.* **2017**, *17*, 1858–1871. [[CrossRef](#)] [[PubMed](#)]
137. Su, Y.; Liu, S.; Guan, Y.; Xie, Z.; Zheng, M.; Jing, X. Renal clearable Hafnium-doped carbon dots for CT/Fluorescence imaging of orthotopic liver cancer. *Biomaterials* **2020**, *255*, 120110. [[CrossRef](#)]
138. Zhang, M.; Ju, H.; Zhang, L.; Sun, M.; Zhou, Z.; Dai, Z.; Zhang, L.; Gong, A.; Wu, C.; Du, F. Engineering iodine-doped carbon dots as dual-modal probes for fluorescence and X-ray CT imaging. *Int. J. Nanomed.* **2015**, *10*, 6943.
139. Zhao, Y.; Hao, X.; Lu, W.; Wang, R.; Shan, X.; Chen, Q.; Sun, G.; Liu, J. Facile preparation of double rare earth-doped carbon dots for MRI/CT/FI multimodal imaging. *ACS Appl. Nano Mater.* **2018**, *1*, 2544–2551. [[CrossRef](#)]
140. Jiao, M.; Wang, Y.; Wang, W.; Zhou, X.; Xu, J.; Xing, Y.; Chen, L.; Zhang, Y.; Chen, M.; Xu, K. Gadolinium doped red-emissive carbon dots as targeted theranostic agents for fluorescence and MR imaging guided cancer phototherapy. *Chem. Eng. J.* **2022**, *440*, 135965. [[CrossRef](#)]
141. Jiang, Q.; Liu, L.; Li, Q.; Cao, Y.; Chen, D.; Du, Q.; Yang, X.; Huang, D.; Pei, R.; Chen, X.; et al. NIR-laser-triggered gadolinium-doped carbon dots for magnetic resonance imaging, drug delivery and combined photothermal chemotherapy for triple negative breast cancer. *J. Nanobiotechnol.* **2021**, *19*, 64. [[CrossRef](#)]
142. Xu, N.; Du, J.; Yao, Q.; Ge, H.; Li, H.; Xu, F.; Gao, F.; Xian, L.; Fan, J.; Peng, X. Precise photodynamic therapy: Penetrating the nuclear envelope with photosensitive carbon dots. *Carbon N. Y.* **2020**, *159*, 74–82. [[CrossRef](#)]
143. Jia, Q.; Ge, J.; Liu, W.; Liu, S.; Niu, G.; Guo, L.; Zhang, H.; Wang, P. Gold nanorod@ silica-carbon dots as multifunctional phototheranostics for fluorescence and photoacoustic imaging-guided synergistic photodynamic/photothermal therapy. *Nanoscale* **2016**, *8*, 13067–13077. [[CrossRef](#)] [[PubMed](#)]
144. Su, H.; Liao, Y.; Wu, F.; Sun, X.; Liu, H.; Wang, K.; Zhu, X. Cetuximab-Conjugated iodine doped carbon dots as a dual fluorescent/CT probe for targeted imaging of lung cancer cells. *Colloids Surf. B Biointerfaces* **2018**, *170*, 194–200. [[CrossRef](#)] [[PubMed](#)]
145. Sun, S.; Chen, J.; Jiang, K.; Tang, Z.; Wang, Y.; Li, Z.; Liu, C.; Wu, A.; Lin, H. Ce6-Modified carbon dots for multimodal-imaging-guided and single-NIR-laser-triggered photothermal/photodynamic synergistic cancer therapy by reduced irradiation power. *ACS Appl. Mater. Interfaces* **2019**, *11*, 5791–5803. [[CrossRef](#)] [[PubMed](#)]
146. Ji, B.; Wei, M.; Yang, B. Recent advances in nanomedicines for photodynamic therapy (PDT)-driven cancer immunotherapy. *Theranostics* **2022**, *12*, 434. [[CrossRef](#)]
147. Chen, C.; Wu, C.; Yu, J.; Zhu, X.; Wu, Y.; Liu, J.; Zhang, Y. Photodynamic-Based combinatorial cancer therapy strategies: Tuning the properties of nanoplatfrom according to oncotherapy needs. *Coord. Chem. Rev.* **2022**, *461*, 214495. [[CrossRef](#)]
148. Hao, Y.; Chung, C.K.; Yu, Z.; Huis In 't Veld, R.V.; Ossendorp, F.A.; Ten Dijke, P.; Cruz, L.J. Combinatorial therapeutic approaches with nanomaterial-based photodynamic cancer therapy. *Pharmaceutics* **2022**, *14*, 120. [[CrossRef](#)]
149. Afanasiev, M.S.; Dushkin, A.D.; Grishacheva, T.G.; Afanasiev, S.S. Photodynamic therapy for early-stage cervical cancer treatment. *Photodiagn. Photodyn. Ther.* **2022**, *37*, 102620. [[CrossRef](#)]
150. Sai, D.L.; Lee, J.; Nguyen, D.L.; Kim, Y.-P. Tailoring photosensitive ROS for advanced photodynamic therapy. *Exp. Mol. Med.* **2021**, *53*, 495–504. [[CrossRef](#)]
151. Zhang, W.; Yu, L.; Jiang, Y.; Guo, C. Phycocyanin-functionalized black phosphorus quantum dots enhance PDT/PTT therapy by inducing ROS and irreparable DNA damage. *Biomater. Sci.* **2021**, *9*, 5302–5318. [[CrossRef](#)] [[PubMed](#)]
152. Hu, X.; Wang, S.; Luo, Q.; Ge, B.; Cheng, Q.; Dong, C.; Xu, J.; Ding, H.; Xu, M.; Tedesco, A.C. Synthesis of Sn nanocluster@ carbon dots for photodynamic therapy application. *Chin. Chem. Lett.* **2021**, *32*, 2287–2291. [[CrossRef](#)]
153. Irmania, N.; Dehvari, K.; Gedda, G.; Tseng, P.; Chang, J. Manganese-Doped green tea-derived carbon quantum dots as a targeted dual imaging and photodynamic therapy platform. *J. Biomed. Mater. Res. Part B Appl. Biomater.* **2020**, *108*, 1616–1625. [[CrossRef](#)]
154. Guo, X.-L.; Ding, Z.-Y.; Deng, S.-M.; Wen, C.-C.; Shen, X.-C.; Jiang, B.-P.; Liang, H. A novel strategy of transition-metal doping to engineer absorption of carbon dots for near-infrared photothermal/photodynamic therapies. *Carbon N. Y.* **2018**, *134*, 519–530. [[CrossRef](#)]

155. Wu, F.; Yue, L.; Su, H.; Wang, K.; Yang, L.; Zhu, X. Carbon dots@ platinum porphyrin composite as theranostic nanoagent for efficient photodynamic cancer therapy. *Nanoscale Res. Lett.* **2018**, *13*, 357. [[CrossRef](#)]
156. Chen, S.; Jia, Q.; Zheng, X.; Wen, Y.; Liu, W.; Zhang, H.; Ge, J.; Wang, P. PEGylated carbon dot/MnO<sub>2</sub> nanohybrid: A new pH/H<sub>2</sub>O<sub>2</sub>-driven, turn-on cancer nanotheranostics. *Sci. China Mater.* **2018**, *61*, 1325–1338. [[CrossRef](#)]
157. Li, M.; Yu, C.; Hu, C.; Yang, W.; Zhao, C.; Wang, S.; Zhang, M.; Zhao, J.; Wang, X.; Qiu, J. Solvothermal conversion of coal into nitrogen-doped carbon dots with singlet oxygen generation and high quantum yield. *Chem. Eng. J.* **2017**, *320*, 570–575. [[CrossRef](#)]
158. Huang, P.; Lin, J.; Wang, X.; Wang, Z.; Zhang, C.; He, M.; Wang, K.; Chen, F.; Li, Z.; Shen, G. Light-Triggered theranostics based on photosensitizer-conjugated carbon dots for simultaneous enhanced-fluorescence imaging and photodynamic therapy. *Adv. Mater.* **2012**, *24*, 5104–5110. [[CrossRef](#)]
159. Bai, Y.; Zhao, J.; Wang, S.; Lin, T.; Ye, F.; Zhao, S. Carbon dots with absorption red-shifting for two-photon fluorescence imaging of tumor tissue pH and synergistic phototherapy. *ACS Appl. Mater. Interfaces* **2021**, *13*, 35365–35375. [[CrossRef](#)]